PERIODICO di MINERALOGIA
established in 1930

DIPARTIMENTO
DI SCIENZE DELLA TERRA

SAPIENZA
UNIVERSITÀ DI ROMA

An International Journal of
Mineralogy, Crystallography, Geochemistry,
Ore Deposits, Petrology, Volcanology
and applied topics on Environment, Archaeometry and Cultural Heritage

Paleotethys-related water-rocks interactions in gabbros of the Anarak ophiolite (Central Iran): constraints from mineralogy and geochemistry

Mahmoud Ahmadi, Mortaza Sharifi *, Ghodrat Torabi

Department of Geology, University of Isfahan, Azadi Square, 8174673441, Isfahan, Iran

ARTICLE INFO

Submitted: December 2019
Accepted: February 2020
Available on line: April 2020

* Corresponding author:
m.sharifi@sci.ui.ac.ir

DOI: 10.2451/2020PM16607

How to cite this article:
Ahmadi M. et al. (2020)
Period. Mineral. 89, 147-169

ABSTRACT

The Anarak Paleozoic ophiolite with nearly east-west trend is located in the western part of the Central-East Iranian Microcontinent (CEIM). There are some leucocratic gabbros which are found as stocks and dykes that cross-cut the Anarak ophiolite. The studied gabbros are composed of clinopyroxene, amphibole, biotite, plagioclase, chlorite, epidote, garnet, sphene, apatite, prehnite, calcite, rutile, magnetite and ilmenite.

Presence of a very high amount of hydrous minerals in the studied rocks reveal high activity of H2O in the involved fluids. Chemical characteristics of the Anarak gabbros show that residue minerals are garnet, amphibole and plagioclase. Major and trace element characteristics of the studied rocks are consistent with the magma that was formed by partial melting of a garnet-bearing amphibolite.

These hydrous phases are possible products of the reaction between oceanic crust and the fluids of seawater derivation. Ingression of seawater through the oceanic crust and its downward penetration into the upper mantle caused the dissolution of a large amount of Ca and alkali components. At the lower parts of the oceanic crust, Ca added to the studied gabbros and produced new Ca-rich minerals.

The Anarak samples show geochemical signatures of melts derived from a subducted oceanic slab. Distinct trace-element signatures show the similarity of the studied gabbros to adakite-like rocks.

According to the age and location, it is suggested that the primary magma of the Anarak gabbros should be created by partial melting of Paleo-Tethys subducting oceanic crust.

Keywords: Paleozoic; water-rock interaction; gabbro; Anarak ophiolite; Central Iran.

INTRODUCTION

Hydrothermal circulation plays an important role in the chemical change and transformation of the oceanic crust (Alt et al., 1993). It is considered to be main mechanism of heat and chemical process in the oceanic lithosphere (e.g. Ballard et al., 1981; Crane et al., 1988; Fouquet, 1997; McCollom and Shock, 1998; Hart et al., 1999; Rebay et al., 2015; Rizzo et al., 2018). Davis and Elderfield (2004) suggested that the fluids of seawater derivation can reach and affect the base of sheeted dykes and uppermost plutonic section. However, the recent studies (e.g. Python et al., 2007, 2011; Akizawa et al., 2011; Akizawa and Arai, 2014; Arai and Akizawa, 2014; Torabi et al., 2017) extended the depth of seawater circulation to the upper mantle parts.

The oxygen and strontium isotopic data of the lower gabbros of Oman ophiolite (McCulloch et al., 1981; Lanphere, 1981; Gregory and Taylor, 1981) indicate seawater circulation at high temperatures. The strontium isotope analyses of the crustal of Oman

ophiolite (Kawahata et al., 2001), show an increase in the temperature of hydrothermal metamorphism. The temperature raised from lower greenschist facies in the basalts to amphibolite facies in the gabbros.

Diopsidite (Python et al., 2007; Akizawa and Arai, 2014), rodingite (Python et al., 2007) and hornblendite (Torabi et al., 2017) are possible products of the water-rock interactions in mantle peridotites, gabbroic dykes and uppermost mantle peridotites, respectively. The diopsidites are described as the footprint of the very high-temperature circulation of seawater (>800 °C), that leached the plagioclase-rich rocks (Python et al., 2011). Rodingites are interpreted as calcium-rich, SiO_2-undersaturated rocks, composed of Ca-Al and Ca-Mg silicates, formed by Ca-metasomatism of gabbroic dykes (e.g. Capedri et al., 1978; Schandl et al., 1989; O'Hanley et al., 1992; Schandl and Mittwede, 2001; Koutsovitis et al., 2008; Tsikouras et al., 2009; Ferrando et al., 2010; Li et al., 2010; Python et al., 2011). In the eastern part of CEIM (Naein ophiolite), the hornblendites reported as dykes, formed by circulation of high-temperature fluids of seawater derivation within the Naein oceanic lithosphere and uppermost mantle (Torabi et al., 2017).

Iran is a mosaic of microcontinents and ophiolites which were mainly accreted in the borders of continental terranes. The Paleozoic Anarak ophiolite (Central Iran) has been intruded by leucocratic gabbro suites, which are found as stocks and dykes. The studied gabbros show mineralogical and geochemical evidences of water-rock interactions which induced by seawater-derived fluids. In this study, the petrography, mineral chemistry and petrological aspects of the gabbros are investigated.

GEOLOGICAL SETTING

The Anarak area is located in the western part of CEIM, a subdivision of structural units of Iran in the Alpine-Himalayan orogenic belt (Figure 1). The Anarak ophiolite is one of the Paleozoic metaophiolites which are located in the western part of the CEIM and it is considered as a remnant of the Paleo-Tethys oceanic crust (Stampfli and Borel, 2004; Bagheri and Stampfli, 2008; Torabi, 2011). This ophiolite consists of mantle peridotite, serpentinized mantle peridotites, cumulates, gabbros, basic and ultrabasic dykes, pyroxenite, glaucophane-bearing metabasalts (blueschist), rodingite, listwaenite and trondhjemites (Sharkovski et al., 1984; Torabi et al., 2011). The Anarak ophiolite resemble the lherzolitic ophiolite type (Torabi, 2009). This ophiolite unconformably covered by Liassic continental molassic deposits, which later metamorphosed (Late Paleozoic metamorphic rocks) (Figure 2). The mantle peridotites of Anarak ophiolite have undergone a high degree of serpentinization (Torabi, 2009; Torabi et al., 2011).

The petrology and structural geology of the Anarak area has been studied by Sharkovski et al. (1984), Diefenbach et al. (1986), Stampfli and Borel (2004), Bagheri (2007), Bagheri and Stampfli. (2008) and Torabi et al. (2011). They have considered this ophiolite as belonging the Paleozoic ophiolites of Iran based on geological, geochemical and geodynamic investigations. Bagheri (2007) revealed that the Anarak-Jandaq terrane belongs to the tectonic evolution of the Palaeo-Tethys Ocean.

Bagheri and Stampfli (2008) proposed a new name "Variscan accretionary complex" for the most widely distributed metamorphic rocks related to the Anarak and Jandaq metamorphic complexes. The Variscan accretionary complex is a thick and fine grain siliciclastic sequence with ophiolitic remnants, consisting of gabbro and basalts with a supra-subduction geochemical signature (Bagheri and Stampfli, 2008). Zanchi et al. (2009) concluded that the Nakhlak-Anarak units represents an arc-trench system developed during the Cimmerian orogeny in central Iran. Torabi (2012) demonstrate that the late Permian trondhjemites of Anarak ophiolite crystallized by a magma originated from the melting of the Anarak subducted oceanic crust.

^{40}Ar-^{39}Ar dating on muscovite of the Anarak metamorphic rocks constraints the ages of metamorphism about 319.0±1.6 to 333.9±1.9 Ma (Bagheri, 2007), comparable to the Variscan age from central Asia and Eurasia. Furthermore, ^{40}Ar-^{39}Ar dating method of sodic amphibole in Anarak blueschist show the age of 285.4±1.65 Ma, pointing to late Permian metamorphism of the primary pillow lavas (Bagheri, 2007).

U-Pb dating on zircon of trondhjemitic intrusions emplaced into the Anarak ophiolite gives an age of 262.3±1.0 Ma (Late Permian) (Bagheri, 2007), which recommends that the trondhjemitic magmatism happened after the formation of blueschists in the Anarak ophiolite.

The compositions and chemical characteristics of the Anarak ophiolite is similar to the Bayazeh ophiolite, a member of Paleozoic ophiolites in the western part of the CEIM, that obducted through the closure of the Paleo-Tethys ocean from Early to Late Paleozoic time (Nosouhian et al., 2019).

In addition to the cumulate gabbros existing in the Anarak ophiolite, there are some leucocratic gabbro intrusions in the form of stocks and dykes, which are cross-cutting the Anarak ophiolite rock units (Figure 2). The thickness of the dykes varies from 1 to 5 meters and the diameter of the stocks is up to 150 meters. The outcrops of these gabbros, which have emplaced into the mantle peridotites of Anarak ophiolite, can be seen in the south of Chah-Shoor Nickel mine, south of Rasoor polymetallic mine, south of Chah-Gorbeh mountain and south of Nakhlak Pb-Zn mine (Figure 3).

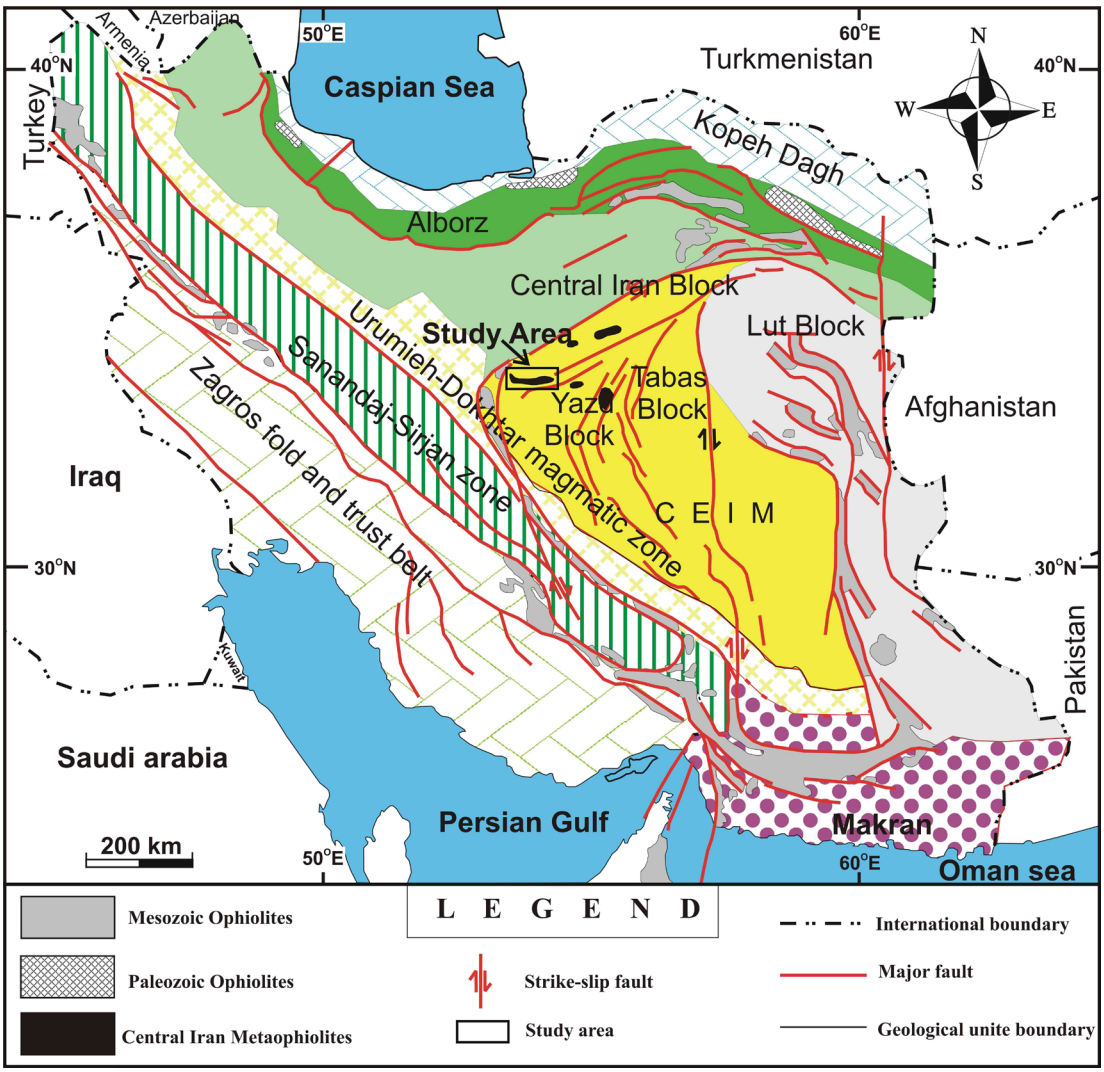

Figure 1. Major structural units of Iran, location of the ophiolites of Iran and the study area. CEIM (Central-East Iranian Microcontinent); Modified after Torabi (2013) and Saccani et al. (2013) slightly changed.

The studied gabbros have lighter color than the mantle peridotites and other ophiolitic rock units and therefore can be easily distinguished from the other rocks of the ophiolite assemblages (Figure 3).

ANALYTICAL METHODS

Major elements analyses of minerals were taken using a wavelength-dispersive electron probe microanalyzer (EPMA) (JEOL JXA-8800R) at the Earth Science Department of the Kanazawa University (Japan). Accelerating voltage was 15 kV and probe current was 15 nA. All elements were analyzed with 40 seconds counting times and the probe diameter was 3 μm. The chemical compositions of coexisting minerals in the gabbros of Anarak ophiolite carried out by EPMA are summarized in Tables 1-5. The Fe^{3+} content of minerals derived using stoichiometric criteria (Droop, 1987). The Mg# and Fe# calculated as [Mg/ (Mg+Fe^{2+})] and [Fe^{2+}/(Fe^{2+}+Mg)] atomic ratio of minerals, respectively.

Trace elements analyses of clinopyroxene and actinolite were determined by laser ablation system (193 nm ArF Excimer) coupled to an Agilent 7500s ICP-MS system at the Earth Science Department of the Kanazawa University, Japan (Morishita et al., 2005a, 2005b). According to the method proposed by Morishita et al. (2005a), samples were spot ablated for 40s at a 10Hz repetition rate in an ultrahigh purity He-N2 atmosphere using a 110 μm beam and laser energy of 8 J/cm^2 per pulse. The trace elements compositions of coexisting minerals in the studied rocks carried out by LA-ICP-MS are showed in Table 6.

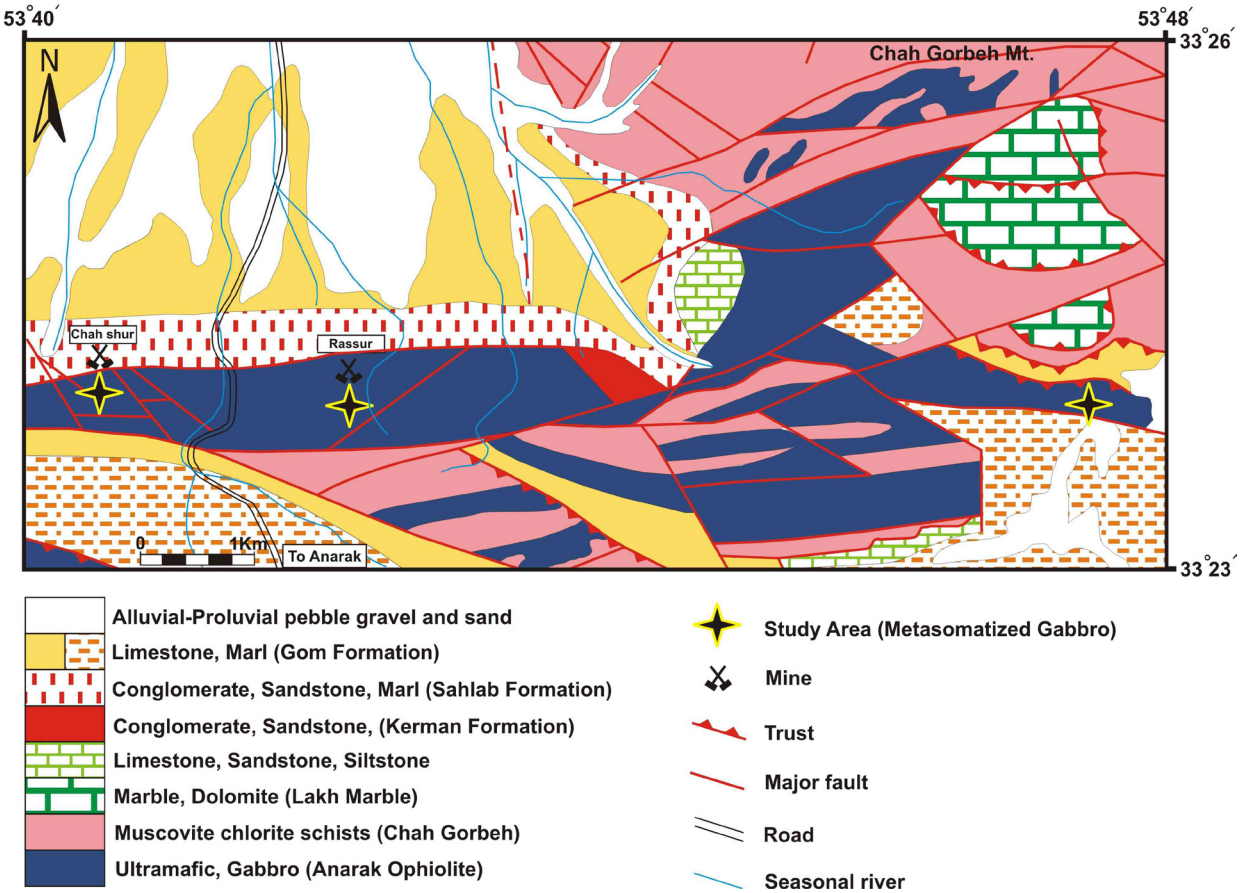

Figure 2. Simplified geological map of the Anarak region (Isfahan province, Central Iran). Modified after Sharkovski et al. (1984) and Zanchi et al. (2009) slightly changed.

The major and trace element compositions of the studied gabbros were carried out by a combination of Inductively Coupled Plasma Emission Spectrometry (ICP-ES) and Inductively Coupled Plasma Mass Spectrometry (ICP-MS) methods at the Acme lab, Canada. Whole rock geochemical data of the gabbros from Anarak ophiolite are presented in Table 7. Mineral abbreviations are taken from Whitney and Evans (2010).

PETROGRAPHY AND MINERAL CHEMISTRY

The gabbros of Anarak ophiolite are massive and medium to coarse-grained leucocratic gabbros. In thin sections, they have mainly granoblastic, poikiloblastic and nematoblastic textures. Most of the primary minerals of the studied gabbros are modified due to water-rock interaction processes. Sometimes the remnants of the primary texture can be observed. According to petrography study (Ahmadi et al., 2018), the Anarak gabbros composed of clinopyroxene, amphibole, plagioclase, biotite, chlorite, epidote, garnet, sphene, apatite, prehnite, calcite, rutile, magnetite and ilmenite (Figure 4).

The SiO_2, Al_2O_3, TiO_2 and Mg# of clinopyroxenes contents vary from 48.13 to 55.54 wt%, 0.01 to 6.78 wt%, 0.01-2.13 wt% and 0.85-0.94, respectively (Table 1). According to Wo-En-Fs classification diagram of clinopyroxenes (Morimoto et al., 1988), most of clinopyroxenes plots in Augite and Diopside fields (Figure 5a, 5b).

Based on the amphibole classification graph (Leake et al., 1997), the studied amphiboles are actinolite, tremolite and magnesiohornblende in composition (Figure 5c). They have TiO_2<0.50 wt% and Mg#=0.45 to 0.93 (Table 2).

Microprobe analyses of plagioclases reveal that they are albite to oligoclase (Ab_{90-99}) in composition (Deer et al., 1992) (Table 3; Figure 5d).

According to the biotite classification diagram (Rieder et al., 1998), the studied biotites are phlogopite in composition (Figure 5e). Phlogopites have Mg# 0.73 to 0.87 and Al_2O_3 values of 13.94 to 14.72 wt% (Table 3). Based on the classification diagram of chlorites

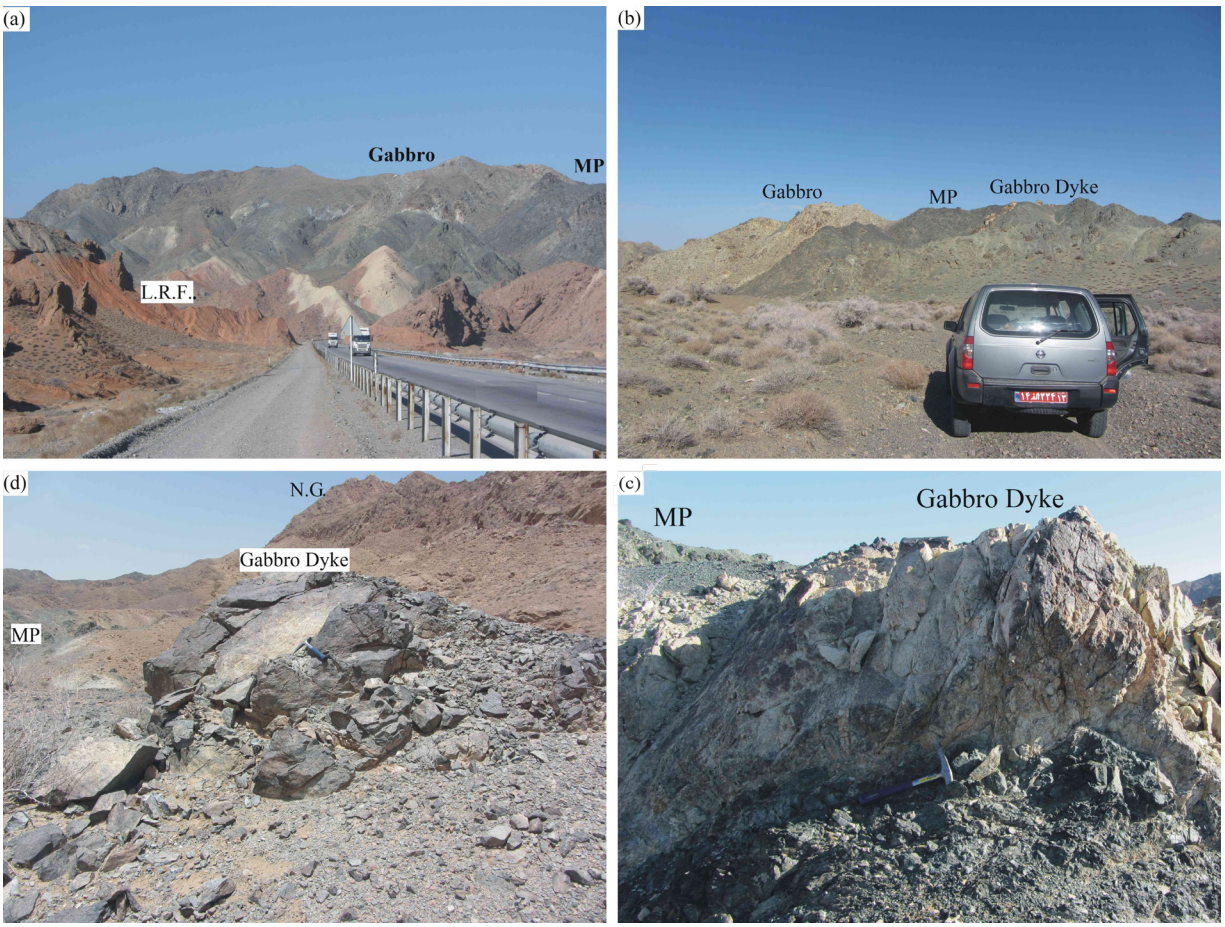

Figure 3. Field photograph of the gabbros of Anarak ophiolite: (a) gabbro stock in the south of Chah-shoor mine (view to N). (b) Outcrop of the studied gabbros in the south of Rasour mine (view to NW). (c) Gabbro dyke in the south of Chah-Gorbeh Mountain (view to E). (d) Gabbro dyke from the south of Nakhlak mine (view to NW). (MP: Mantle Peridotites, L.R.F.: Lower Red Formation, N.G.: Nakhlak Group).

(Hey, 1954), the Anarak chlorites are pycnochlorite and penninite in composition (Figure 5f) with Mg#=0.65-0.91 (Table 4). Calcite and dolomite are carbonate minerals in the studied rocks, which occur as irregular veins, indicating their late-stage origin.

The "pistacite" component [Ps# (X_{Fe}=100*Fe^{3+}/(Fe^{3+} +Al)] of Epidotes from the gabbros of Anarak ophiolite are 19.7-28.5%. The garnets are grossular-almandine with a composition of Grs=70.18-78.02% and Alm=21.38-27.95%. The sphenes of studied gabbros have contents of 39.67-39.90 (wt%) Al_2O_3 and 0.06-0.88 (wt%) TiO_2 (Table 5).

The clinopyroxene origin determination graph (Berger et al., 2005) indicates that clinopyroxenes of the studied gabbros have igneous nature (Figure 6a). The composition of igneous clinopyroxene (Halama et al., 2003; Berger et al., 2005) and metamorphic clinopyroxene (Berger et al., 2005) added to figure 6a for comparison. All amphiboles in Ti-Si binary plot (Figure 6b) present metamorphic nature (Veblen and Ribbe, 1982). Biotites in ternary diagram of Nachit et al. (2005) plotted on the re-equilibrated biotites limited area (Figure 6c).

The LA-ICP-MS analyses of clinopyroxenes (Table 6) and Chondrite-normalized REE patterns (Figure 7a) (the elemental concentrations are taken from Sun and McDonough, 1989) show that clinopyroxenes are more enriched in REE compared to chondrite (5 to 20 times). They are enriched in LREEs and depleted in HREEs [$(Ce/Yb)_n$=9.73-11.75]. The clinopyroxenes of the studied rocks exhibit slight negative and positive Eu anomalies (Figure 7a). They are characterized by low Sm/Yb ratio (1.82-3.16) and low Yb contents (0.77-1.24). Chondrite-normalized REE patterns (Figure 7a) (the elemental concentrations are taken from Sun and McDonough, 1989) of the analyzed actinolite exhibit depletion in LREE, enrichment in HREE and clear positive Eu anomaly. The composition of clinopyroxene from oceanic gabbros (Nimis and Vannucci, 1995) and calculated equilibrium

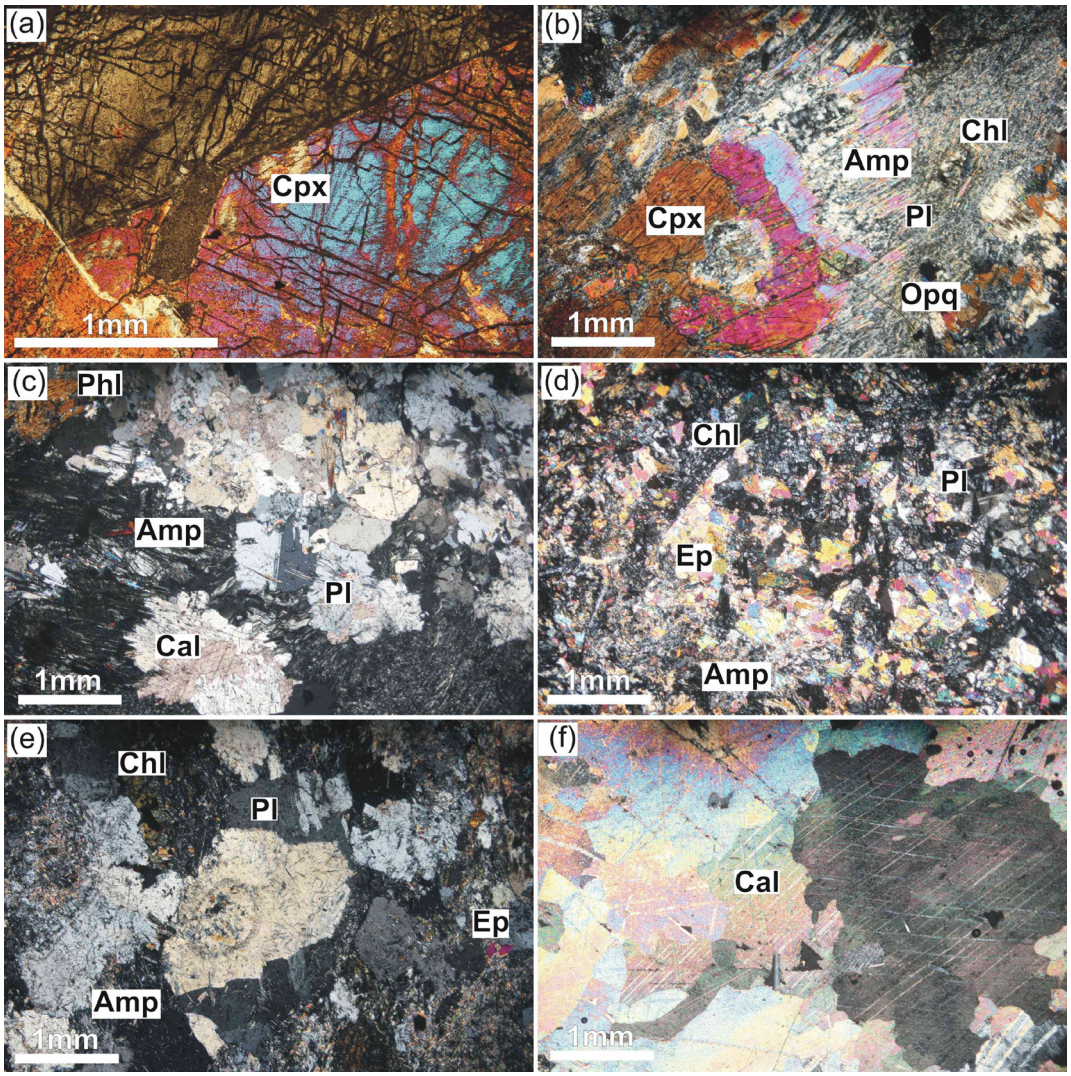

Figure 4. Photomicrographs of the gabbros of Anarak ophiolite. (a) Fresh phenocrysts of clinopyroxene as primary mineral (XPL). (b) Presence of clinopyroxene, amphibole, sodic plagioclase, chlorite and opaque in the studied samples (XPL). (c) Amphibole, sodic plagioclase and chlorite with carbonate as secondary minerals (XPL). (d) High amounts of hydrous minerals (amphibole, biotite, chlotite and epidite). (XPL). (e) High abundance of sodic plagioclase and lack of calcic plagioclase (XPL). (f) Carbonate crystalization in the Anarak samples (XPL).

melt coexisting with clinopyroxene were added to Figure 7a for comparison.

Primitive mantle-normalized multi-element spider diagram of clinopyroxenes (Figure 7b) (the elemental concentrations are taken from McDonough and Sun, 1995) show that they have negative anomalies of large-ion lithophile elements (LILEs) (Rb, Ba and Sr), high field strength elements (HFSEs) (Nb, Ta, Zr, Ti) and Pb. In the primitive mantle-normalized multi-elements spidergram (Figure 7b), the analyzed actinolite shows positive anomalies of LILEs, HFSE, Eu and Pb and negative anomalies of LREE, Zr and Ti.

WHOLE ROCK CHEMISTRY

The geochemical analyses of the gabbros of Anarak ophiolite show that SiO_2 contents vary from 37.99 to 51.06 wt% and MgO contents vary from 7.24 to 28.15 wt% (Table 7). The Al_2O_3, TiO_2 and CaO contents of analyzed rocks are 6.92 to 19.06 wt%, 0.25 to 1.49 wt% and 4.21 to 18.08 wt%, respectively (Table 7). The studied gabbros have contents of 0.07 to 1.94 (wt%) K_2O and 0.02 to 4.02 (wt%) Na_2O (Table 7).

The variations in Na_2O values in different samples, the formation of secondary minerals and chemical composition of plagioclase point to the effect of fluids of seawater derivation in the studied rocks (Torabi,

Table 1. Representative chemical composition of clinopyroxenes (wt.%) from the gabbros of the Anarak ophiolite and their calculated structural formula.

Sample	38	39	40	41	42	44	45	51	53	54	62	133-1	133-3	133-5	133-7
Mineral	Cpx	Cpx	Cpx	Cpx	Cpx	Cpx	Cpx	Cpx	Cpx	Cpx	Cpx	Cpx	Cpx	Cpx	Cpx
SiO_2	50.93	50.75	49.83	49.72	49.91	49.76	48.98	49.72	50.45	49.94	49.57	50.85	50.62	50.35	50.70
TiO_2	0.86	0.89	1.43	1.41	1.38	1.55	1.65	1.05	0.84	1.04	1.57	0.89	1.25	1.26	1.20
Al_2O_3	3.94	4.28	4.97	5.06	4.81	5.07	5.19	4.80	4.25	4.48	5.05	3.60	4.04	4.18	3.78
Cr_2O_3	0.19	0.30	0.27	0.25	0.32	0.24	0.22	0.42	0.88	0.74	-	0.10	0.15	0.14	0.09
FeO*	5.26	5.32	6.56	5.88	6.00	7.41	5.99	6.78	5.20	7.28	6.75	5.45	5.97	5.78	5.53
MnO	0.13	0.12	0.14	0.16	0.14	0.18	0.14	0.15	0.12	0.13	0.15	0.09	0.13	0.10	0.13
MgO	15.34	14.86	14.75	12.22	14.19	15.40	14.09	15.29	14.63	16.41	14.73	14.27	14.69	14.65	14.45
CaO	22.72	23.06	21.67	23.04	22.65	19.61	22.83	20.88	22.97	20.05	21.56	23.98	22.73	23.23	23.54
Na_2O	0.43	0.49	0.50	0.50	0.55	0.50	0.48	0.47	0.63	0.37	0.49	0.37	0.40	0.43	0.51
K_2O	-	-	-	-	0.12	-	-	-	-	0.01	-	-	0.01	0.02	0.01
NiO	0.03	0.02	0.01	0.01	-	-	0.01	0.01	0.03	0.03	-	0.02	0.02	0.03	0.01
Total	99.83	100.09	100.14	100.25	100.07	99.72	99.58	99.58	100.00	100.47	99.88	99.62	100.01	100.16	99.97
Structural Formula Base on the 6 Oxygens															
Si	1.87	1.86	1.83	1.88	1.84	1.84	1.81	1.84	1.85	1.83	1.83	1.88	1.87	1.85	1.87
Ti	0.02	0.03	0.04	0.04	0.04	0.04	0.05	0.03	0.02	0.03	0.04	0.03	0.04	0.04	0.03
Al	0.17	0.19	0.22	0.23	0.21	0.21	0.19	0.22	0.18	0.19	0.22	0.16	0.18	0.18	0.16
Cr	0.01	0.01	0.01	0.01	0.01	0.01	0.01	0.01	0.03	0.02	-	-	-	-	-
Fe^{2+}	0.09	0.09	0.13	0.19	0.11	0.18	0.10	0.13	0.08	0.12	0.04	0.10	0.07	0.10	0.10
Fe^{3+}	0.07	0.07	0.07	-	0.08	0.05	0.08	0.08	0.08	0.11	0.07	0.06	0.05	0.08	0.07
Mn	-	-	-	0.01	-	0.01	-	0.01	-	-	0.01	-	-	-	-
Mg	0.84	0.81	0.81	0.69	0.78	0.85	0.78	0.84	0.80	0.90	0.81	0.79	0.81	0.80	0.79
Ca	0.89	0.91	0.85	0.93	0.89	0.78	0.91	0.83	0.90	0.79	0.85	0.95	0.90	0.92	0.93
Na	0.03	0.04	0.04	0.04	0.04	0.04	0.03	0.03	0.05	0.03	0.04	0.03	0.03	0.03	0.04
K	-	-	-	-	0.01	-	-	-	-	-	-	-	-	-	-
Sum	4.00	4.00	4.00	4.00	3.99	4.00	4.00	4.00	4.00	4.00	4.00	4.00	4.00	4.00	4.00
Mg#	0.93	0.93	0.90	0.93	0.91	0.87	0.94	0.91	0.97	0.93	0.90	0.90	0.89	0.93	0.92
X_{Wo}	47.06	48.05	45.69	51.47	48.01	41.76	48.35	43.90	48.38	41.19	45.45	49.80	47.42	48.20	48.97
X_{En}	44.23	43.10	43.28	37.99	41.83	45.63	41.52	44.72	42.88	46.93	43.21	41.22	42.65	42.28	41.83
X_{Fs}	8.72	8.86	11.04	10.54	10.16	12.62	10.13	11.39	8.74	11.88	11.35	8.99	9.94	9.52	9.20

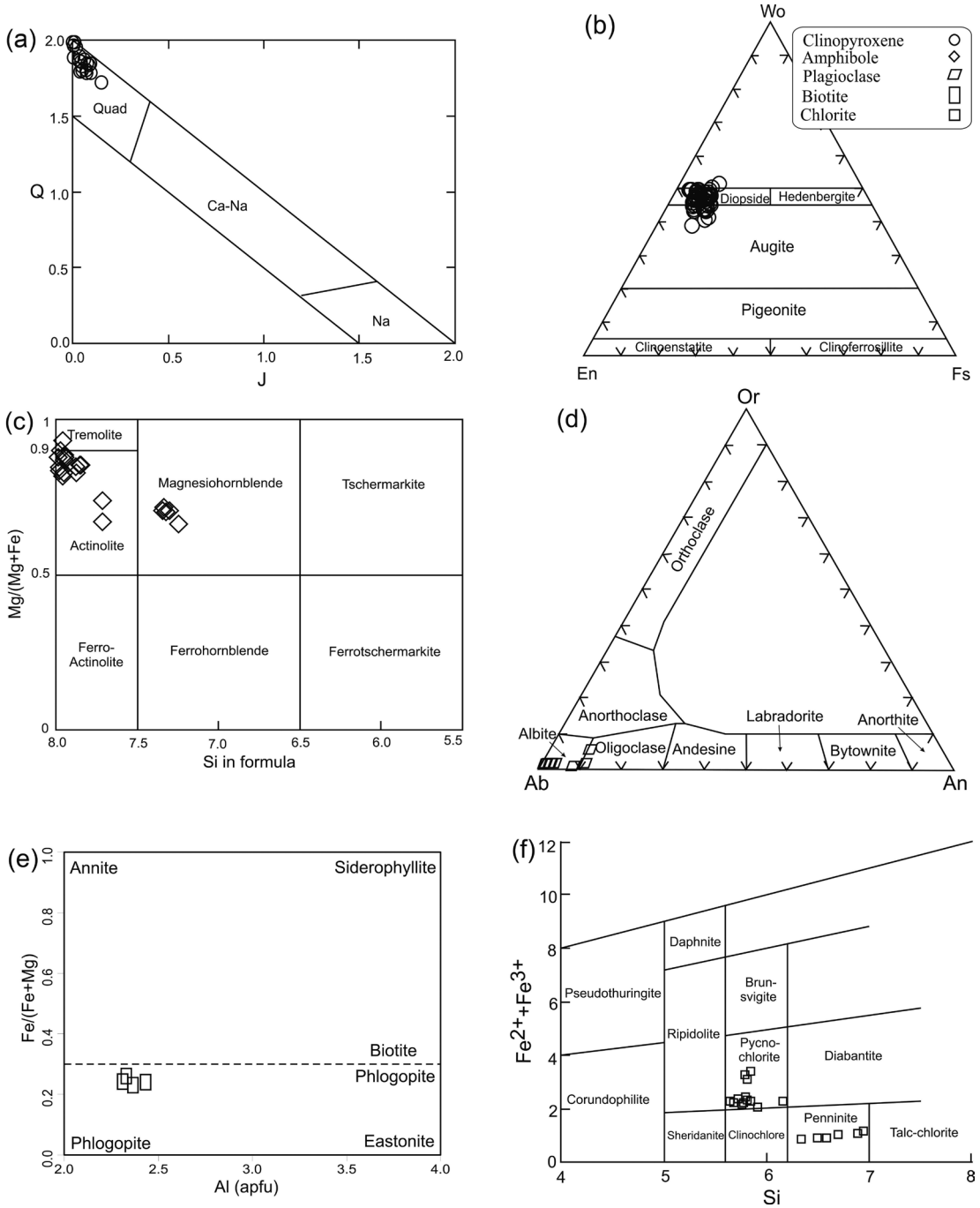

Figure 5. Classification diagrams and chemical graphs of the gabbros of Anarak ophiolite minerals (a) Q vs J Diagram (Morimoto et al., 1988). (b) Clinopyroxene of the Anarak samples are augite to diopside in composition at Clinopyroxene classification triangle (Morimoto et al., 1988). (c) The amphiboles show tremolite, actinolite and magnesiohornblende composition (Leake et al., 1997). (d) Plagioclases are albite to oligoclase in composition (Deer et al., 1992). (e) Biotites classification diagram after Rieder et al. (1998). (f) Classification diagram for chlorite from studied gabbros according to Hey (1954).

2012; Nosouhian et al., 2019). High Al_2O_3 indicating a metaluminous parental melt (Shand, 1943) and low K_2O contents indicating low to medium potassium magma series (Le Maitre et al., 1989).

Chondrite-normalized REE patterns (Figure 8a) show that the studied gabbros enriched in LREE, fractionated and depleted in HREE and no positive or negative Eu anomaly (the elemental concentrations are taken from Sun

Table 2. Representative chemical composition of amphiboles (wt%) from the gabbros of the Anarak ophiolite and their calculated structural formula.

Sample	47	48	56	59	68	70	75	77	80	88	90	95	97	129-4	129-5	129-11
Mineral	Amp	Amp	Amp	Amp	Amp	Amp	Amp	Amp	Amp	Amp	Amp	Amp	Amp	Amp	Amp	Amp
SiO_2	56.77	56.60	55.80	57.08	55.97	56.25	56.87	53.59	57.39	57.34	57.55	57.08	57.10	50.72	50.88	50.93
TiO_2	-	0.01	-	0.01	-	0.01	-	0.06	-	-	0.01	0.02	0.03	0.65	0.70	0.74
Al_2O_3	0.37	0.73	0.88	0.35	1.78	1.22	0.67	2.90	0.54	0.12	0.07	0.10	0.09	6.05	6.28	5.91
Cr_2O_3	-	-	-	-	-	-	-	-	-	0.16	0.15	-	0.05	0.01	0.04	-
FeO*	8.17	8.67	8.41	7.08	7.06	6.99	7.82	13.04	7.88	6.30	4.41	6.12	6.14	11.20	11.20	10.78
MnO	0.23	0.23	0.18	0.16	0.15	0.17	0.18	0.26	0.24	0.15	0.27	0.14	0.12	0.28	0.28	0.31
MgO	18.94	18.37	18.22	19.85	18.98	19.53	19.09	14.84	19.18	20.49	21.69	20.39	20.27	15.02	14.76	15.13
CaO	12.21	11.47	11.30	12.33	12.53	12.57	11.64	12.63	11.81	12.04	12.46	12.33	12.11	12.94	12.87	12.44
Na_2O	0.71	1.08	1.22	0.56	0.81	0.60	1.02	0.59	0.81	0.84	0.64	0.67	0.78	1.01	0.86	1.03
K_2O	0.07	0.06	0.08	0.05	0.06	0.03	0.07	0.05	0.07	0.04	0.08	0.04	0.07	0.12	0.15	0.11
NiO	0.07	0.05	0.06	0.06	0.07	0.09	0.10	0.01	0.08	0.02	0.04	0.07	0.05	0.01	0.02	0.01
Total	97.53	97.27	96.15	97.51	97.40	97.46	97.45	97.96	98.00	97.50	97.36	96.96	96.82	98.00	98.03	97.39
Structural Formula Base on the 23 Oxygens																
Si	7.99	8.00	7.98	7.99	7.86	7.89	7.99	7.71	8.02	8.00	7.99	8.01	8.02	7.29	7.30	7.34
Ti	-	-	-	-	-	-	-	0.01	-	-	-	-	-	0.07	0.08	0.08
Al	0.06	0.12	0.15	0.06	0.29	0.20	0.11	0.49	0.09	0.02	0.01	0.02	0.02	1.03	1.06	1.00
Cr	-	-	-	-	-	-	-	-	-	0.02	0.02	-	0.01	-	0.01	-
Fe^{2+}	0.96	1.03	1.01	0.83	0.83	0.82	0.92	1.57	0.92	0.74	0.51	0.72	0.72	1.35	1.34	1.30
Fe^{3+}	-	-	-	-	-	-	-	-	-	-	-	-	-	-	-	-
Mn	0.03	0.03	0.02	0.02	0.02	0.02	0.02	0.03	0.03	0.02	0.03	0.02	0.01	0.03	0.03	0.04
Mg	3.98	3.87	3.88	4.14	3.97	4.09	4.00	3.18	3.99	4.27	4.49	4.27	4.24	3.22	3.16	3.25
Ca	1.84	1.74	1.73	1.85	1.89	1.89	1.75	1.95	1.77	1.80	1.85	1.83	1.82	1.99	1.98	1.92
Na	0.19	0.30	0.34	0.15	0.22	0.16	0.28	0.16	0.22	0.23	0.17	0.18	0.21	0.28	0.24	0.29
K	0.01	0.01	0.02	0.01	0.01	0.01	0.01	0.01	0.01	0.01	0.01	0.01	0.01	0.02	0.03	0.02
Ni	0.01	-	-	-	0.01	0.01	0.01	-	0.01	-	-	0.01	-	-	-	-
Sum	15.07	15.09	15.12	15.05	15.10	15.09	15.09	15.12	15.05	15.10	15.09	15.07	15.08	15.28	15.22	15.23
Mg#	0.81	0.79	0.79	0.83	0.82	0.83	0.81	0.67	0.81	0.88	0.90	0.86	0.85	0.71	0.70	0.71

Table 3. Representative chemical composition of plagioclase and biotite (wt%) from the gabbros of the Anarak ophiolite and their calculated structural formula.

Sample	22	37	85	129-1	129-2	129-6	129-10	133-8	Sample	92	99	101
Mineral	Pl	Pl	Pl	Pl	Pl	Pl	Pl	Pl	Mineral	Bt	Bt	Bt
SiO_2	68.45	68.47	68.44	68.06	67.01	65.00	66.39	69.03	SiO_2	36.17	35.39	35.24
TiO_2	-	0.01	-	-	-	-	-	-	TiO_2	4.45	5.60	5.32
Al_2O_3	19.42	19.70	19.27	19.45	20.44	21.25	20.90	19.17	Al_2O_3	13.94	14.73	14.21
Cr_2O_3	-	-	-	-	0.02	-	-	0.01	Cr_2O_3	-	-	-
FeO*	0.06	0.05	0.02	0.03	0.04	0.12	0.15	0.01	FeO*	12.32	11.13	11.21
MnO	-	-	-	0.01	0.01	0.03	0.02	-	MnO	0.21	0.23	0.20
MgO	0.01	-	-	-	-	0.13	-	-	MgO	19.29	20.06	20.51
CaO	0.01	0.04	0.03	0.34	1.42	2.22	2.03	0.07	CaO	0.02	0.06	0.03
Na_2O	11.32	11.43	11.24	11.60	10.64	10.03	10.39	11.55	Na_2O	0.03	0.01	0.02
K_2O	0.01	0.03	0.02	0.04	0.07	0.97	0.05	0.04	K_2O	7.95	7.85	7.63
NiO	-	0.01	0.01	-	0.01	-	-	-	NiO	0.05	0.04	0.05
Total	99.28	99.73	99.02	99.57	99.64	99.75	99.93	99.87	Total	94.43	95.09	94.43
Structural Formula Base on the 8 Oxygens									Base on the 22 Oxygens			
Si	3.00	2.99	3.01	2.99	2.94	2.88	2.92	3.01	Si	5.13	4.96	4.98
Ti	-	-	-	-	-	-	-	-	Ti	0.47	0.59	0.56
Al	1.00	1.01	1.00	1.01	1.06	1.11	1.08	0.99	Al	2.33	2.43	2.36
Cr	-	-	-	-	-	-	-	-	Cr	-	-	0.02
Fe^{2+}	-	-	-	-	-	-	-	-	Fe^{2+}	1.46	1.31	1.32
Fe^{3+}	-	-	-	-	-	-	0.01	-	Fe^{3+}	-	-	-
Mn	-	-	-	-	-	-	-	-	Mn	0.02	0.03	0.02
Mg	-	-	-	-	-	0.01	-	-	Mg	4.08	4.20	4.32
Ca	-	-	-	0.02	0.07	0.11	0.10	-	Ca	-	0.01	-
Na	0.96	0.97	0.96	0.99	0.91	0.86	0.89	0.98	Na	0.01	-	0.01
K	-	-	-	-	-	0.06	-	-	K	1.44	1.40	1.37
Ni	-	-	-	-	-	-	-	-	Sum	14.95	14.93	14.96
Sum	4.98	4.98	4.97	5.00	4.98	5.02	4.99	4.98	Fe#	0.26	0.24	0.23
X_{Ab}	99.80	99.60	99.80	98.20	92.70	84.30	89.90	99.60	Mg#	0.74	0.76	0.77
X_{An}	0.10	0.20	0.10	1.60	6.90	10.30	9.80	0.30				
X_{Or}	0.10	0.20	0.10	0.20	0.40	5.40	0.30	0.10				

and McDonough, 1989). They present fractionated REE patterns characterized by low HREE (Yb=0.31 to 1.12 ppm), Y contents (3.8 to 11.2 ppm) and high La/Yb ratios (4.20 to 13.11). The studied gabbros are characterized by 1.5 to 38 times REE enrichment in comparison to chondrite.

In the primitive mantle-normalized diagram (the elemental concentrations are taken from McDonough and Sun, 1995) (Figure 8b), the concentrations in trace elements of the studied gabbros show large heterogeneity. The studied gabbros show enrichment in LILE (e.g. Cs, Rb, Ba, U and Pb) and HFSE (e.g. Nb, Ta, Zr and P). Pb shows a prominent positive anomaly, while Sr and Ti display both positive and negative anomalies.

Comparing the average composition of gabbros of the Anarak ophiolite with the unaltered late Paleozoic oceanic gabbros (Tsygankov et al., 2016) reveal enrichment in FeO, MgO, CaO and Na_2O and depletion in SiO_2 and REEs of the studied gabbros. Considerable high loss on ignition (LOI) values (3.4-9.7 wt%) are due to presence of hydrous minerals. The large variations in the geochemical analyses values may be explained by differences in reaction intensity or magmatic fractionation.

Table 4. Representative chemical composition of chlorite and calcite (wt%) from the gabbros of the Anarak ophiolite and their calculated structural formula.

Sample	31	32	35	43	55	58	73	82	83	86	87	Sample	46	36
Mineral	Chl	Chl	Chl	Chl	Chl	Chl	Chl	Chl	Chl	Chl	Chl	Mineral	Cal	Cal
SiO_2	28.69	28.55	28.82	28.30	29.58	28.97	28.56	28.59	28.92	28.98	29.13	SiO_2	-	-
TiO_2	-	0.01	-	-	-	-	-	0.01	-	-	0.02	TiO_2	-	-
Al_2O_3	18.36	19.16	18.91	20.03	19.51	19.29	20.04	19.62	20.02	18.85	19.65	Al_2O_3	-	0.03
Cr_2O_3	0.04	0.13	0.02	0.05	-	-	-	-	-	-	0.09	Cr_2O_3	-	-
FeO*	20.09	19.24	18.37	13.82	13.16	13.55	14.28	14.23	13.76	13.95	14.17	FeO*	0.12	0.08
MnO	0.30	0.29	0.23	0.19	0.17	0.17	0.23	0.22	0.17	0.18	0.20	MnO	0.15	0.01
MgO	20.51	20.51	21.64	24.48	24.37	24.59	23.90	24.05	24.25	24.49	24.18	MgO	0.16	0.05
CaO	0.01	0.03	0.03	0.02	0.08	0.05	0.02	0.02	0.01	0.07	0.11	CaO	54.71	54.68
Na_2O	-	0.01	0.01	0.01	-	0.01	-	-	-	0.01	-	Na_2O	-	-
K_2O	-	0.01	0.01	-	0.01	-	-	0.01	0.01	-	-	K_2O	-	0.08
NiO	0.04	0.03	0.03	0.12	0.03	0.15	0.17	0.17	0.16	0.12	0.14	NiO	-	-
Total	88.04	87.97	88.07	87.02	86.91	86.76	87.19	86.91	87.29	86.66	87.69	Total	55.14	54.93
Structural Formula Base on the 28 Oxygens												Base on the 1 Oxygens		
Si	5.84	5.79	5.81	5.65	5.84	5.78	5.72	5.72	5.74	5.81	5.77	Si	-	-
Ti	-	-	-	-	-	-	-	-	-	-	-	Ti	-	-
Al	4.40	4.58	4.49	4.71	4.54	4.54	4.63	4.63	4.68	4.45	4.58	Al	-	-
Cr	0.01	0.02	-	0.01	-	-	-	-	-	-	0.02	Cr	-	-
Fe^{2+}	3.42	3.26	3.10	2.31	2.28	2.26	2.39	2.38	2.28	2.34	2.35	Fe^{2+}	-	0.01
Mn	0.51	0.05	0.04	0.03	0.03	0.03	0.04	0.04	0.03	0.03	0.03	Fe^{3+}	-	-
Mg	6.22	6.20	6.50	7.28	7.18	7.32	7.18	7.18	7.18	7.32	7.14	Mn	-	0.01
Ca	-	0.01	0.01	-	0.02	0.01	-	-	-	0.02	0.02	Mg	-	0.01
Na	-	-	0.01	-	-	0.01	-	-	-	-	-	Ca	0.99	1.00
K	-	-	-	-	-	-	-	-	-	-	-	Na	-	-
Ni	-	-	-	0.01	-	0.02	0.02	0.02	0.02	0.01	0.02	K	-	-
Sum	19.95	19.91	19.95	19.99	19.89	19.94	19.96	19.96	19.91	19.96	19.92	Ni	-	-
Fe#	0.35	0.34	0.32	0.24	0.24	0.24	0.25	0.25	0.24	0.24	0.25	Sum	1.00	1.02
Mg#	0.65	0.66	0.68	0.76	0.76	0.76	0.75	0.75	0.76	0.76	0.75			

DISCUSSION

Petrogenesis of gabbros

Despite the effect of water-rock interaction processes in the studied rocks, the distribution of immobile elements such as Al, Ti, HFSEs and REEs are regular, suggests that these values are reliable. During magma crystallization, LREEs prefer to enter in the plagioclase structure more than in the clinopyroxene structure.

The mineral chemistry of primary igneous minerals such as clinopyroxene in altered and metamorphosed rocks can display the signatures of the primary magma (Leterrier et al., 1982). The noteworthy, composition of clinopyroxene is highly sensitive to variations in pressure, temperature, and melt-water content (e.g. Mollo et al., 2013, 2018). It was calculated that the melt composition coexisting with clinopyroxene (Wood and Blundy, 1997; Sun and Liang, 2012) can be used to recognize the nature of the original magma and its processes (Figures 7a, 8a).

On the basis of SiO_2 versus Al_2O_3 binary diagram (Le Bas, 1962), the clinopyroxenes of the studied gabbros are represented by sub-alkaline series (Figure 9a). The Ti versus Al graph which separates clinopyroxenes into calc-alkaline and tholeiitic magma types (Leterrier et al., 1982), shows that the studied rocks exhibit calc-alkaline composition (Figure 9b). As shown in Figure 9c (Winchester and Floyd, 1977), the clinopyroxenes of the studied samples show a basic composition.

The diagrams discriminating between adakitic and

Table 5. Representative chemical composition of epidote, garnet and sphene (wt%) from the gabbros of the Anarak ophiolite and their calculated structural formula.

Sample	23	29	30	60	61	69	71	74	78	Sample	66	72	Sample	18	92
Mineral	Ep	Ep	Ep	Ep	Ep	Ep	Ep	Ep	Ep	Mineral	Grt	Grt	Mineral	Sph	Sph
SiO_2	38.17	38.21	38.62	38.73	38.60	38.47	38.43	38.25	38.28	SiO_2	37.93	38.38	SiO_2	30.71	30.46
TiO_2	0.07	0.11	0.01	0.32	0.02	0.12	0.04	0.07	0.02	TiO_2	0.08	0.12	TiO_2	39.67	39.91
Al_2O_3	27.01	25.89	25.82	25.74	25.74	26.33	25.94	25.51	25.84	Al_2O_3	25.46	25.86	Al_2O_3	0.88	0.06
Cr_2O_3	-	0.16	0.10	-	0.01	0.01	-	-	-	Cr_2O_3	-	-	Cr_2O_3	-	0.07
FeO*	7.56	8.43	8.98	9.13	9.13	8.32	9.17	9.49	9.24	FeO*	8.91	8.62	FeO*	0.18	0.81
MnO	0.11	0.19	0.13	0.07	0.07	0.07	0.06	0.09	0.10	MnO	0.05	0.04	MnO	-	0.03
MgO	-	-	0.02	0.04	0.04	0.03	-	-	0.01	MgO	0.03	-	MgO	0.01	0.06
CaO	23.71	23.80	23.91	23.79	23.79	23.77	23.55	23.73	24.01	CaO	23.86	23.79	CaO	29.24	28.78
Na_2O	0.01	-	0.01	-	-	-	0.01	-	0.02	Na_2O	-	-	Na_2O	0.05	0.01
K_2O	-	-	0.01	-	-	-	-	-	0.01	K_2O	-	-	K_2O	-	-
NiO	-	0.01	-	0.01	-	-	0.01	-	-	NiO	-	-	NiO	0.01	0.01
Total	96.64	96.81	97.61	97.83	97.40	97.11	97.20	97.14	97.53	Total	96.32	96.82	Total	100.75	100.21
Structural Formula Base on the 12.5 Oxygens										Base on the 12 Oxygens			Base on the 5 Oxygens		
Si	3.00	3.03	3.04	3.04	3.05	3.03	3.03	3.03	3.02	Si	3.00	3.02	Si	1.00	1.00
Ti	-	0.01	-	0.02	-	0.01	-	-	-	Ti	-	-	Ti	0.97	0.98
Al	2.50	2.42	2.39	2.38	2.36	2.44	2.41	2.38	2.40	Al	2.37	2.40	Al	0.03	-
Fe^{3+}	0.50	0.50	0.53	0.54	0.59	0.49	0.54	0.56	0.55	Fe^{2+}	0.59	0.57	Cr	-	-
Cr	-	0.01	0.01	-	-	-	-	-	-	Mn	-	-	Fe^{2+}	0.01	0.02
Mn	0.01	0.01	0.01	-	-	0.01	-	0.01	0.01	Mg	-	-	Fe^{3+}	-	-
Mg	-	-	-	-	-	-	-	-	-	Ca	2.02	2.01	Mn	-	-
Ca	1.99	2.02	2.02	2.00	1.98	2.01	1.99	2.01	2.03	Na	-	-	Mg	-	-
Na	-	-	-	-	-	-	-	-	-	Sum	8.00	8.00	Ca	1.02	1.01
K	-	-	-	-	-	-	-	-	-	X_{Alm}	22.52	22.01	Na	-	-
Ni	-	-	-	-	-	-	-	-	-	X_{Grs}	77.22	77.87	K	-	-
Sum	8.00	7.99	7.99	7.98	7.98	7.99	7.98	7.99	8.01	X_{Pyr}	0.13	0.01	Ni	-	-
										X_{Sps}	0.13	0.11	Sum	3.02	3.02

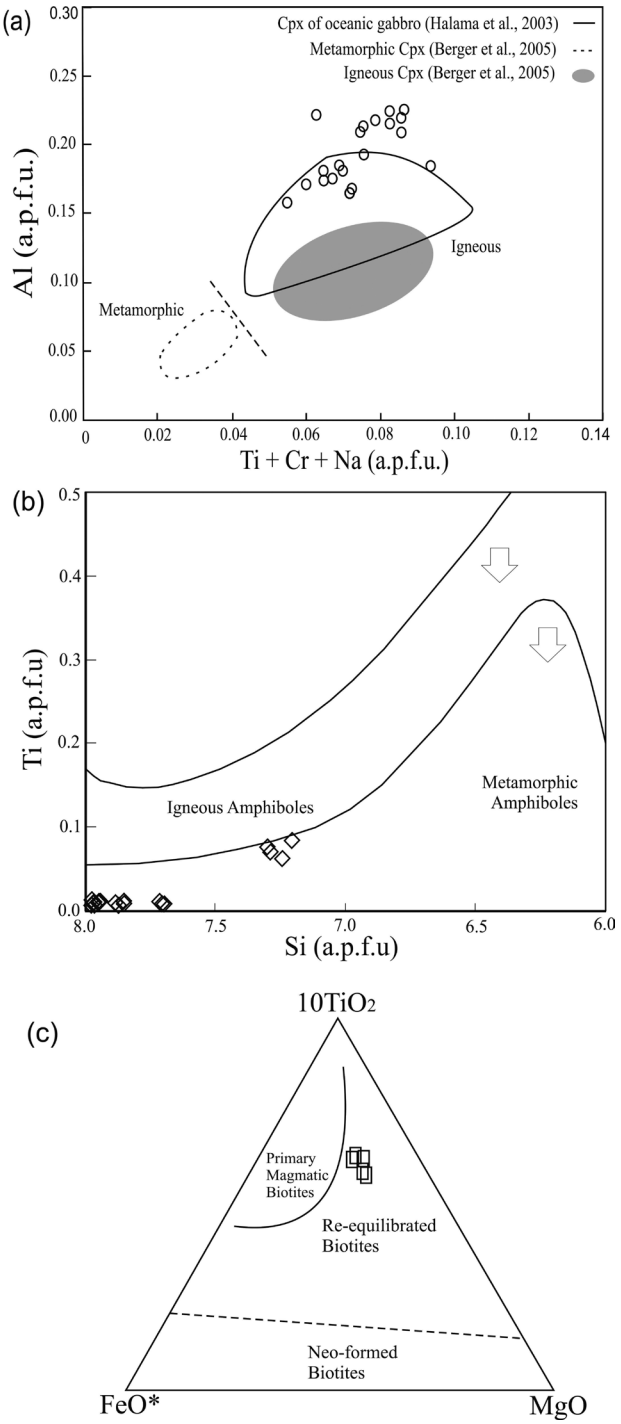

Figure 6. (a) Al vs (Ti+Cr+Na) diagram of clinopyroxenes of the studied samples (Berger et al., 2005). The composition of igneous clinopyroxene are from Halama et al. (2003), Berger et al. (2005) and the composition of metamorphic clinopyroxene are from Berger et al. (2005). (b) Amphibole types and position of the studied amphiboles in the Ti vs Si diagram (Veblen and Ribbe, 1982). (c) Chemical composition of biotites of the Anarak gabbros in the $10TiO_2$-FeO*-MgO ternary diagram of Nachit et al. (2005). Symbols are as shown in Figure 5.

normal arc calc-alkaline rocks compositions (Drummond and Defant, 1990) show that the studied gabbros have adakitic nature (Figure 10a). Calc-alkaline arc rocks that show extreme LREE enrichment, very high Sr/Y ratios, and low Yb and heavy REE concentrations, but have different major element concentrations from adakites, are known as "adakite-like" rocks (Kolb et al., 2013).

The enriched LREE patterns of Anarak samples can be explained by partial melting of a source leaving a refractory phase assemblage with various proportions of clinopyroxene, hornblende and garnet. Deplated HREEs and low values of Y of the studied samples show that garnet or hornblende retained at the site of partial melting (Torabi, 2012). In addition, the high-Al content may have resulted from the removal of hornblende from the melt as a residual phase at the source or as a fractionation product (Barker and Arth, 1976; Barker, 1979; Coolican et al., 2000).

Presence of Ti-rich phase such as rutile, ilmenite and phlogopite show that the negative Ti anomalies of studied clinopyroxenes in the primitive mantle-normalized diagram may be related to residual titanium phases in a subduction-related magma (Stalder et al., 1998). In addition, high Ti mobility in hydrothermal fluid at a relatively low pressure cannot be expected (Antignano and Manning, 2008).

Water-rock interaction

Petrography and geochemical studies indicate that the gabbros of Anarak ophiolite interacted with seawater-derived fluids and as a result, most of the primary minerals transformed into secondary minerals. Clinopyroxene is only igneous mineral in the studied rocks. Water-rock interaction has changed the primary calcic plagioclase to secondary sodic ones. The effect of alteration process in the calcic plagioclase resulted in the formation of actinolite, albite, calcite, epidote and chlorite. Presence of sodic plagioclase (albite and oligoclase) and lack of calcic ones show that the studied rocks are affected by Na-rich fluids. High degree albitization of plagioclase could reflect excess Na_2O. Consequently, calcic plagioclase has been enriched in Na against seawater-originated fluids to form sodic plagioclase (McCollom and Schock, 1998). In addition, a high abundance of calcic minerals such as actinolite, tremolite, epidote, grossular, sphene, prehnite and calcite reveals that the hydrothermal fluids where Ca rich. Low REE and HFSE contents of amphiboles of Anarak gabbros, suggest amphibole-forming reactions between primary igneous minerals and seawater-derived fluids (Tribuzio et al., 2014).

The presence of a very high amount of hydrous minerals (up to 80 vol%), high LOI values of the analyzed samples (3.40 to 8.70 wt%) and the textural and chemical

Table 6. Microprobe (major elements in wt%) and LA-ICP-MS (trace elements in ppm) analyses of clinopyroxene and amphibole from the gabbros of the Anarak ophiolite.

Sample	304	305	312	314	319	321	324	325
	Cpx	Amp	Cpx	Cpx	Cpx	Cpx	Cpx	Cpx
SiO_2	52.21	57.29	53.62	52.08	50.67	50.64	51.64	51.55
TiO_2	0.57	0.03	0.39	0.70	1.51	1.08	0.78	1.15
Al_2O_3	3.78	1.21	2.57	3.82	4.40	4.74	3.75	3.41
Cr_2O_3	0.40	-	0.19	0.39	0.34	0.76	0.68	0.20
FeO*	4.57	7.17	3.65	3.86	6.01	5.62	5.93	6.34
MnO	0.15	0.17	0.09	0.10	0.09	0.10	0.10	0.13
MgO	15.63	19.41	16.17	15.72	15.48	14.72	17.87	15.46
CaO	22.11	13.05	22.93	22.63	20.68	21.74	19.00	21.11
Na_2O	0.57	0.14	0.37	0.50	0.36	0.45	0.29	0.41
K_2O	0.01	0.02	-	-	-	-	-	-
NiO	0.02	0.04	0.02	0.02	0.01	0.03	0.02	0.02
Total	100.02	98.52	100.00	99.83	99.54	99.87	100.05	99.77
Rb	0.11	0.17	0.01	1.17	0.13	-	0.45	0.01
Sr	34.22	9.93	23.63	37.57	56.10	49.98	38.63	27.17
Y	7.94	0.21	12.46	12.48	12.53	10.46	9.13	9.43
Zr	12.64	0.24	50.04	39.42	27.72	24.92	20.03	39.61
Nb	0.70	0.18	0.06	0.95	0.23	0.42	0.78	0.06
Ba	4.13	2.83	1.72	20.71	0.89	0.05	3.77	0.36
La	2.37	0.01	3.51	3.42	2.37	2.63	2.31	3.29
Ce	8.34	0.04	13.71	12.47	9.52	9.62	7.49	9.51
Pr	1.11	0.01	2.00	1.79	1.68	1.49	1.13	1.43
Nd	5.15	0.03	9.42	8.54	9.35	7.86	5.98	7.41
Sm	1.40	0.02	2.41	2.29	3.09	2.45	1.95	2.28
Eu	0.56	0.02	0.79	0.71	1.06	0.89	0.69	0.81
Gd	1.53	0.02	2.52	2.51	3.37	2.70	2.22	2.42
Tb	0.24	-	0.39	0.40	0.49	0.41	0.34	0.36
Dy	1.62	0.03	2.58	2.51	3.04	2.45	2.13	2.29
Ho	0.31	0.01	0.49	0.49	0.54	0.44	0.38	0.40
Er	0.83	0.02	1.35	1.33	1.30	1.07	0.98	0.98
Tm	0.12	0.01	0.19	0.18	0.17	0.14	0.13	0.13
Yb	0.77	0.03	1.24	1.24	0.98	0.90	0.77	0.81
Lu	0.11	0.01	0.19	0.19	0.13	0.11	0.10	0.11
H	0.52	0.01	1.38	1.01	1.30	0.15	0.84	1.46
Ta	0.03	0.01	0.04	0.15	0.04	-	0.06	0.02
Pb	0.36	0.22	0.42	0.42	0.35	0.05	0.42	0.42
Th	0.26	0.01	0.25	0.36	0.03	-	0.17	0.23
U	0.06	-	0.07	0.09	0.01	-	0.04	0.06

heterogeneity point to the circulation of hydrothermal fluids across the studied rocks.

Hydrothermal fluids were possibly derived from penetrating seawater or dehydration of subducting slabs. Becker et al. (2000) showed that the fluids derived from the dehydration of subducted slabs are strongly enriched in K, Rb, and Ba. The studied gabbros show depletion in Rb that supports seawater origin for the developed fluids

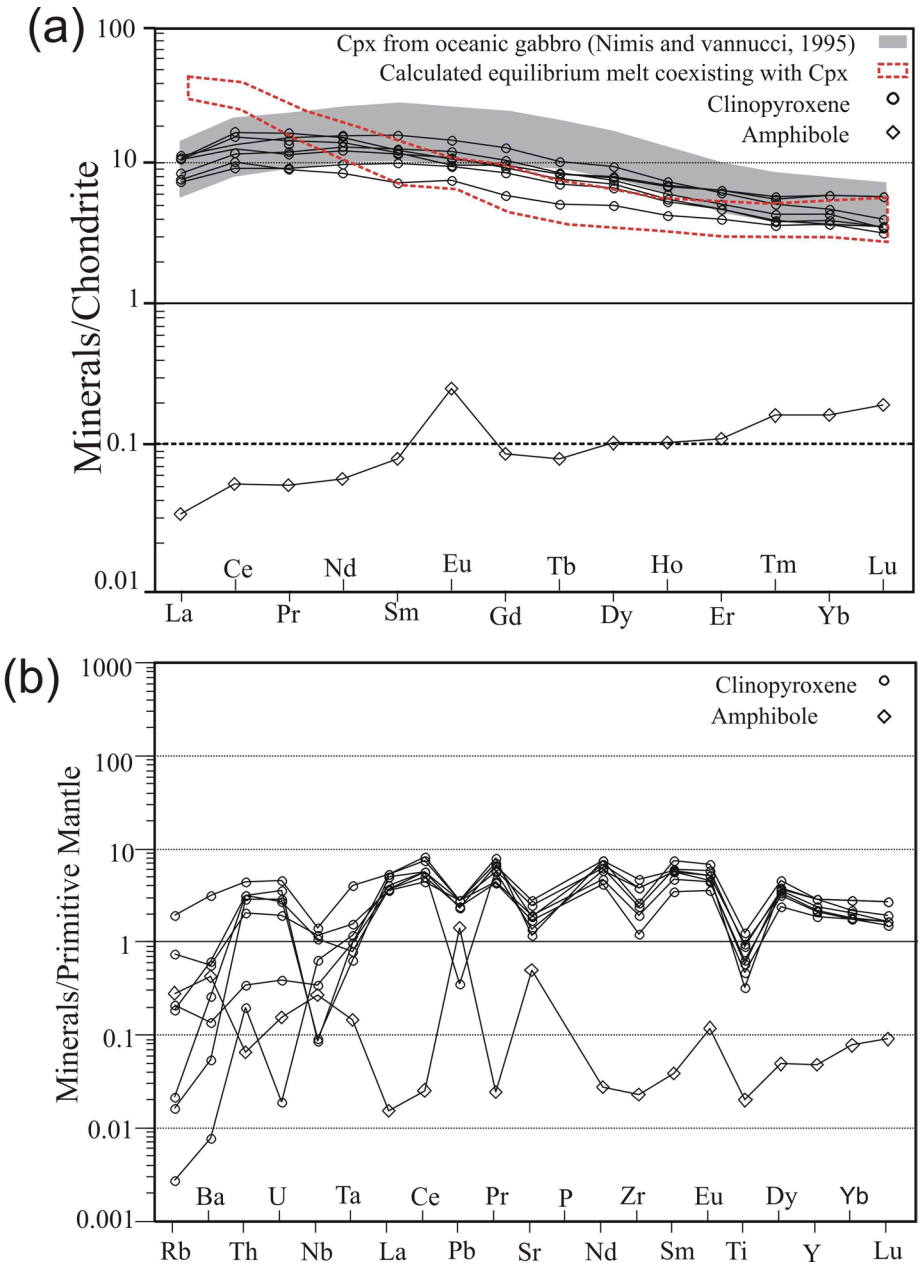

Figure 7. (a) Chondrite-normalized REE patterns of clinopyroxenes and one actinolite of the gabbros of the Anarak ophiolite. The elemental concentrations are from Sun and McDonough (1989). The elemental concentrations of clinopyroxene from oceanic gabbro are from Nimis and Vannucci (1995). Dashed line limited area is the composition of calculated equilibrium melt coexisting with Clinopyroxene. (b) Primitive mantle-normalized multi-element diagram of the analyzed clinopyroxenes and one actinolite of the studied samples. The elemental concentrations are from McDonough and Sun (1995).

rather than subduction-related or slab-derived origin.

Seawater can penetrate down to the mantle at temperatures of about 800 °C, after passing the oceanic crust (Kimball, 1988; Harper, 1985). Interaction of such fluids with the pillow lavas and basaltic dykes cause to the dissolution of a large amount of Ca and alkali-elements in the fluids and these fluids penetrated down to lower crust sections. Chemical reactions of such penetrating hydrothermal fluids possibly transformed the studied rocks into a highly calcic lithology.

Comparing the gabbro of Anarak ophiolite with the unaltered late Paleozoic oceanic gabbros (Tsygankov et al., 2016), indicates that Ca has been increased in the studied gabbros, while Si has been reduced. The conversion of

Table 7. Representative geochemical data of the gabbros of Anarak ophiolite (major elements in wt% and trace elements in ppm).

Sample	A101	A102	A104	A110	A208	A209	A121	A307	A308	A309
SiO_2	45.10	42.37	44.99	47.23	43.28	41.06	47.70	41.03	40.13	37.99
TiO_2	0.69	0.88	1.06	1.09	0.29	0.25	0.41	1.28	1.17	1.49
Al_2O_3	16.74	7.37	10.05	9.85	19.06	17.66	14.63	7.63	7.55	6.92
Fe_2O_3*	5.90	10.14	9.35	8.98	3.17	4.19	5.58	9.40	9.90	10.22
MnO	0.10	0.15	0.14	0.13	0.09	0.10	0.09	0.14	0.14	0.28
MgO	11.83	17.05	15.25	15.31	9.03	12.06	13.47	22.98	24.26	28.15
CaO	8.98	14.58	12.14	11.24	17.72	18.08	9.87	9.91	8.30	4.21
Na_2O	2.29	0.59	1.78	2.11	0.96	0.28	2.18	0.08	0.07	<0.01
K_2O	1.94	0.08	0.10	0.14	0.96	0.14	1.39	0.08	0.11	0.07
Cr_2O_3	0.03	0.14	0.12	0.13	0.10	0.09	0.12	0.15	0.13	0.13
P_2O_5	0.02	0.04	0.05	0.06	<0.01	0.02	0.03	0.15	0.16	0.23
LOI	6.00	6.20	4.60	3.40	5.10	5.80	4.10	6.60	7.50	9.70
Total	99.62	99.59	99.63	99.66	99.76	99.73	99.57	99.43	99.42	99.39
Ni	190.00	469.00	304.00	304.00	216.00	244.00	311.00	548.00	677.00	759.00
Co	42.20	85.60	68.80	65.10	26.10	34.10	37.80	71.10	86.40	83.50
Sc	36.00	42.00	45.00	45.00	25.00	22.00	29.00	26.00	22.00	21.00
V	146.00	178.00	214.00	201.00	88.00	71.00	96.00	145.00	122.00	143.00
Ba	251.00	24.00	23.00	41.00	449.00	59.00	694.00	53.00	63.00	50.00
Zn	29.00	36.00	38.00	45.00	14.00	12.00	22.00	56.00	50.00	30.00
Mo	0.30	0.20	0.30	0.50	0.10	0.40	0.80	0.10	0.30	0.10
As	2.00	<0.50	1.10	0.70	<0.50	<0.50	<0.50	0.70	<0.50	0.80
Rb	20.80	0.90	0.80	1.30	11.80	1.60	19.50	2.80	3.70	2.40
Sr	154.70	206.40	134.70	64.70	49.90	40.50	76.20	30.40	27.90	19.20
Cs	0.70	<0.10	<0.10	<0.10	0.60	<0.10	0.70	0.20	0.30	0.20
Ga	13.10	7.90	9.30	8.90	10.10	10.80	8.80	7.40	7.30	7.60
Ta	0.20	0.20	0.30	0.30	<0.10	<0.10	0.30	0.90	1.00	1.30
Hf	1.00	1.20	1.00	1.30	0.40	0.40	0.60	1.70	1.70	2.40
Zr	25.40	32.50	30.30	43.30	9.60	11.50	24.80	75.80	70.90	104.80
Nb	2.40	3.50	4.80	5.80	0.20	0.90	8.50	14.20	13.30	20.40
Th	0.30	0.30	0.30	0.60	<0.20	<0.20	0.80	1.20	1.10	1.50
U	0.20	-	<0.10	0.20	<0.10	<0.10	0.10	0.30	0.40	0.30
Cu	174.20	58.80	53.20	55.70	15.10	87.70	97.10	31.60	30.10	40.90
Pb	61.30	19.10	41.80	54.60	19.40	4.00	4.00	64.00	20.60	14.40
Y	6.80	8.10	8.50	9.40	4.60	3.80	6.40	9.30	9.00	11.20
La	5.10	4.40	5.50	7.90	3.00	3.40	7.60	12.20	12.40	13.50
Ce	10.20	9.30	12.10	15.30	5.30	6.80	13.70	27.20	25.80	28.90
Pr	1.39	1.36	1.73	2.01	0.71	0.74	1.36	3.21	3.21	3.73
Nd	6.70	6.80	8.40	8.60	3.30	3.00	5.50	13.20	13.30	16.10
Sm	1.65	1.81	2.28	2.47	0.83	0.72	1.09	2.53	2.32	3.16
Eu	0.77	0.68	0.83	0.91	0.51	0.41	0.51	0.61	0.72	0.70
Gd	1.95	2.15	2.41	2.64	1.06	0.87	1.24	2.45	2.33	2.91
Tb	0.27	0.34	0.37	0.42	0.16	0.13	0.20	0.36	0.34	0.45
Dy	1.47	1.70	2.09	2.18	0.80	0.78	1.05	1.93	1.70	2.26
Ho	0.28	0.33	0.39	0.43	0.20	0.15	0.25	0.39	0.39	0.47
Er	0.67	0.97	1.05	1.05	0.54	0.49	0.70	1.01	0.97	1.29
Tm	0.09	0.11	0.12	0.14	0.06	0.06	0.09	0.15	0.14	0.19
Yb	0.50	0.64	0.72	0.87	0.42	0.31	0.66	0.93	0.97	1.12
Lu	0.06	0.09	0.09	0.10	0.05	0.04	0.09	0.13	0.13	0.18

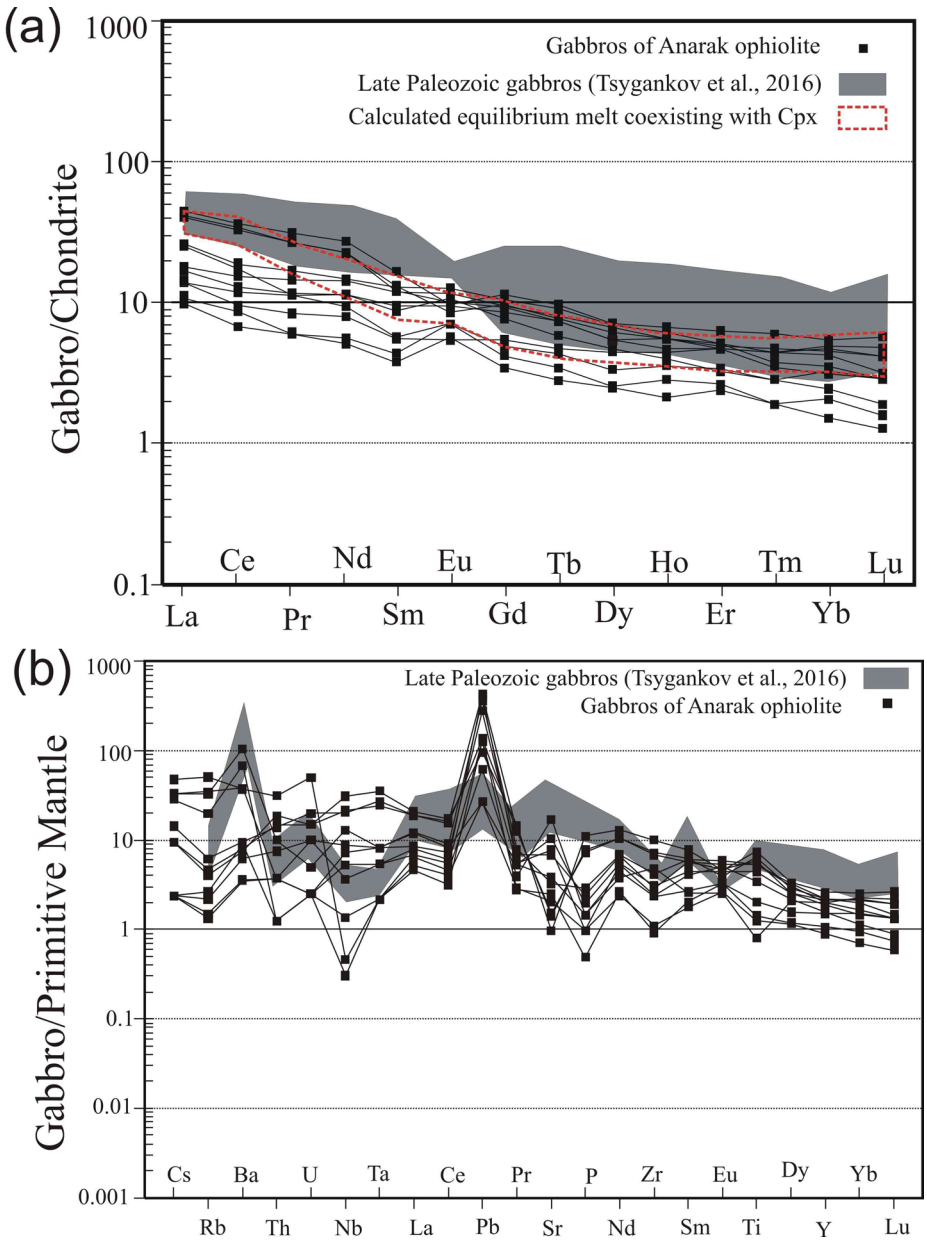

Figure 8. (a) Chondrite-normalized REE patterns of analyzed whole rock and clinopyroxenes of the studied gabbros. The elemental concentrations are from Sun and McDonough (1989). The REE composition of late Paleozoic gabbros are from (Tsygankov et al., 2016). (b) Primitive mantle-normalized multi-element diagram of the analyzed whole rock and clinopyroxenes of the Anarak samples. The elemental concentrations are from McDonough and Sun (1995). The elemental concentrations of late Paleozoic gabbros are from (Tsygankov et al., 2016).

calcic plagioclase to sodic plagioclase which is a common reaction occurring in the oceanic environment (Ramseyer et. al., 1992) is an example for the reduction of Si and increasing of Ca values (equation 1).

$$CaAl_2Si_2O_8+2Na^{+}+4SiO_2 \rightarrow 2NaAlSi_3O_8+Ca^{2+} \quad (1)$$

The high value of Ca in the penetrating fluid cause to the crystallization of the calcium rich minerals such as actinolite, epidote, grossular, prehnite, and calcite. High modal amount of Ca-rich minerals reveal that the hydrothermal fluids leached calcic plagioclase-rich rocks (e.g. pillow lavas, basalts, and dibasic dykes) before reaching to the studied gabbros. All these evidences indicate that the gabbros of Anarak ophiolite interacted with a Ca-rich fluid and were transformed into a highly

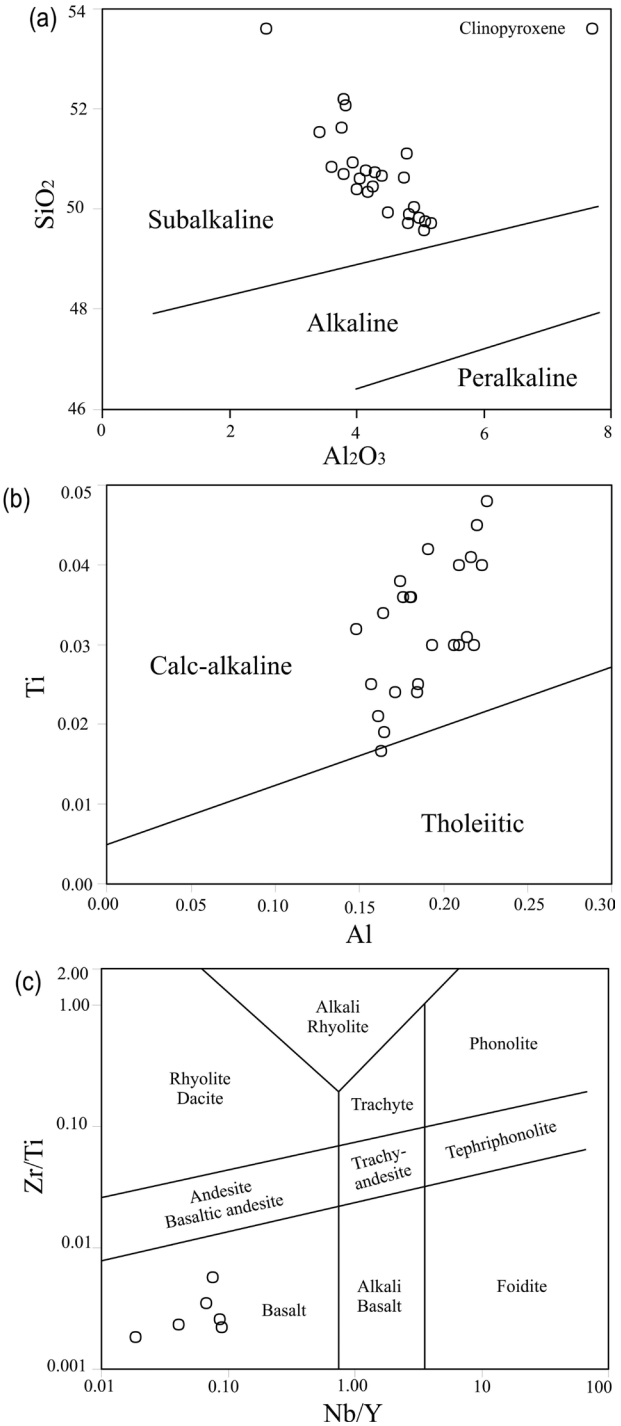

Figure 9. Clinopyroxene discrimination diagrams of the gabbros of Anarak ophiolite. (a) SiO_2-Al_2O_3 diagram of Le Bas (1962) for clinopyroxene of the studied gabbros. All samples stay on sub-alkaline limited are. (b) Plot of Al vs Ti indicates that the Anarak samples are calc-alkaline (Leterrier et al., 1982). (c) Zr/Ti against Nb/Y diagram of Winchester and Floyd (1977). The studied rocks show a basic composition.

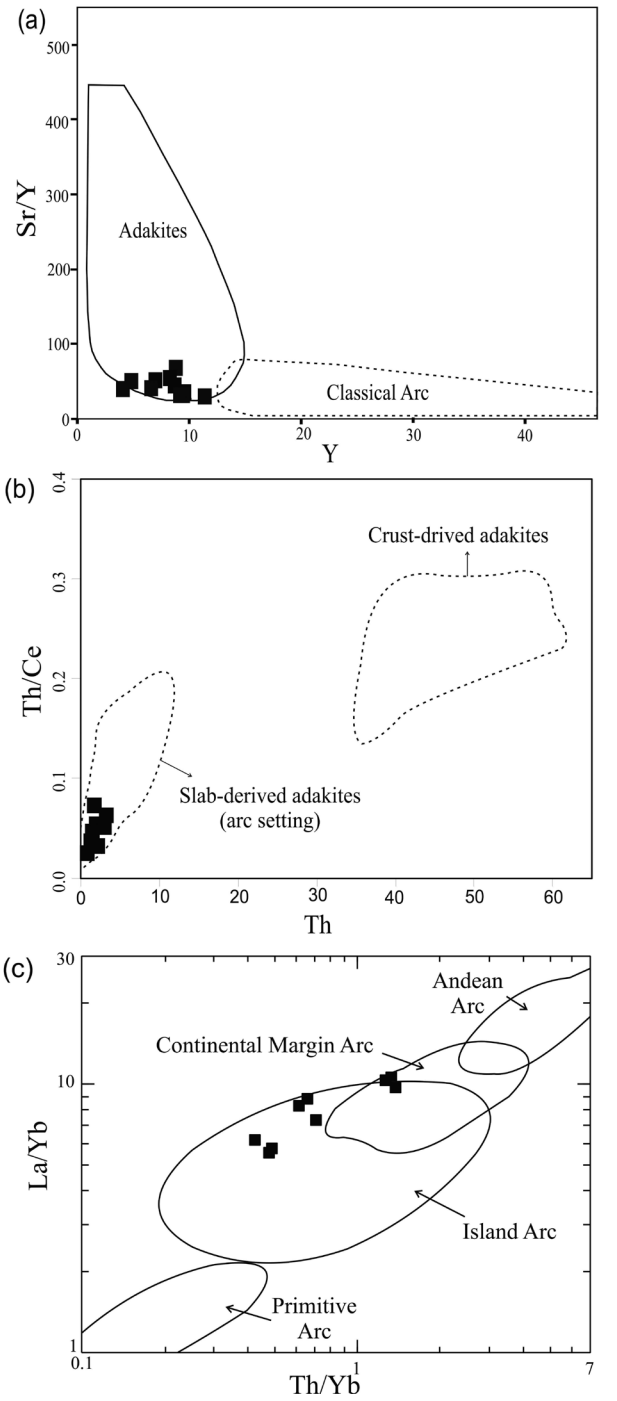

Figure 10. Plots of (a) Sr/Y vs Y (Drummond and Defant, 1990). (b) Th/Ce vs Th diagram of the studied rocks show that the Anarak samples are more consistent with slab-derived adakites in compositions (Wang et al., 2007). (c) La/Yb vs Th/Yb diagram (Condie, 1989) showing the distribution of Anarak samples. Symbol given in Figure 8.

calcic lithology. Cation exchange of alkali elements from hydrothermal fluids lead to the creation of minerals such as amphiboles and albite.

High amounts of sodic plagioclase (albite and oligoclase) indicate that during seawater ingression through the pillow lavas and gabbros, the primary calcic plagioclases are changed to secondary sodic ones (Bosch et al., 2004). The presence of sodic plagioclase and lack of calcic ones show that the studied gabbros should be affected by high-temperature fluids (about 700 °C), because plagioclase is stable down to this temperature (Bosch et al., 2004). Enrichment in LREE, LILE and Pb are the results of circulation of high temperature (up to 700 °C) fluids in the studied gabbros (Ishikawa et al., 2005). This temperature is consistent with the inference from the mineral assemblage and show upper amphibolite facies (Spear, 1981).

Despite the effect of seawater-derived fluids, the distribution of immobile major elements such as Al and Ti, and most of the HFSE and REE is regular, which suggests that they have not undergone significant changes. The wide range of SiO_2 (37.99 to 51.06 wt%) and CaO values (4.21 to 18.08 wt%) (Table 7) in the studied gabbros show that the SiO_2 and CaO content was affected by seawater-derived fluids. These chemical characteristics possibly support seawater origin for the evolved fluids of the gabbros of Anarak ophiolite rather than slab-derived origin. As shown in Figure 10b, the low Th contents and Th/Ce ratios indicate that the compositions of studied rocks are more consistent with slab melting rather than with magma originating in the lower crust (Wang et al., 2007).

Geotectonic setting

The rifting events of Palaeo-Tethys Ocean started in late Ordovician to early Devonian and terminated in the Triassic with Eocimmerian collision (Stampfli and Borel, 2004). At the Kazimovian (300 Ma), Paleotethys mid-ocean fast spreading ridge was rapidly approach to the active margin (Stampfli and Borel, 2004). This will result in ridge failure, oblique subduction of the Paleotethys slab and opening of Permian intra-oceanic back-arc basins (Stampfli and Borel, 2004). Torabi (2011) indicate that the blueschists of the Anarak ophiolite are as remnants of the PaleoTethys suture zone in Central Iran. These unusual tectonic conditions may be prepared the higher geothermal gradients for the production of magmas of Anarak gabbros.

La/Yb versus Th/Yb diagram (Condie, 1989) shows that the corresponding magma of the studied rocks has volcanic-arc geochemical signature (Figure 10c). REE fractionation, HREE depletion and lake of positive or negative Eu anomaly in the studied gabbros are the geochemical signature of melts derived from a subducted oceanic slab. The Anarak gabbros show low Nb/La (0.06-1.51) and high Sr/Sm ratios (6.08-114.03) which are indicative of magmatic affinity with subduction zone settings (Arndt, 2008). Enrichment in LILEs (Cs, Rb and Ba) confirm that the melts derived from a subducted oceanic slab (Figure 8b). Since Ba is more soluble in aqueous fluids than REE, low Ba/La ratios of Anarak gabbros may be explained by addition of sediment components rather than slab fluids (Hanyu et al., 2006).

Lower Sr/Y ratio and a slightly higher HREE content in the Anarak gabbros compared to their Cenozoic counterparts (Martin et al., 2005) indicate that the geothermal gradient in the Paleo-Tethys Oceanic subduction zone and the depth of the Paleo-Tethys Oceanic slab melting lie between their counterparts in the Archean and Cenozoic eras (Zhang et al., 2005).

On the basis of the field outcrops, petrogenesis and paleotectonic evolution of central Iran (Stampfli and Borel, 2004; Bagheri and Stampfli, 2008; Torabi, 2011) including the studied gabbros, it can be suggested that the primary magma of the gabbros of Anarak ophiolite could be created by partial melting of Paleo-Tethys subducted.

CONCLUSION

The leucocratic gabbros of Anarak ophiolite occur as stocks and dykes. They are composed of diopside, augite, actinolite, tremolite, magnesiohornblende, phlogopite, albite, oligoclase, pycnochlorite, penninite, epidote, grossular, sphene, apatite, prehnite, calcite, rutile, magnetite and ilmenite. Clinopyroxenes of studied rocks show high contents of LREE, and low contents of HREE, LILE, HFSE and Pb.

The studied gabbros are sub-alkaline in nature and belong to the calc-alkaline magmatic series. Whole rock chemistry and distinct trace-element signatures show the similarity of studied gabbros to adakite-like rocks. The presence of a very high amount of hydrous minerals shows that this mineral assemblage cannot be formed by igneous processes. They are probably made by the effect of seawater-derived fluids and the primary igneous rocks. Enrichment in LREE, LILE, HFSE and Pb indicate circulation of high temperature (up to 700 °C) fluids in the gabbros of Anarak ophiolite.

REE fractionation, Low HREE and Y depletion of the Anarak samples show melting of a young and hot subducting slab at high pressures. Geochemistry studies show that the residue minerals are garnet, amphibole and plagioclase, indicates that the studied gabbros probably formed by partial melting of an amphibolite bearing garnet.

Major and trace element characteristics of the studied rocks are consistent with the magma that was created by

partial melting of a garnet-bearing amphibolite. According to the age and location of the gabbros of Anarak ophiolite, they may have been generated by partial melting of Paleo-Tethys subducted slab.

ACKNOWLEDGEMENTS

The authors thank the University of Isfahan, Iran for financial supports and Kanazawa University, Japan for laboratory facilities.

REFERENCES

Ahmadi M., Sharifi M., Torabi G., 2018. Petrography and mineral chemistry of metasomatized gabbros from the Anarak Ophiolite. Iranian Journal of Crystallography and Mineralogy 26, 437-454 (In Persian with English abstract).

Akizawa N., Arai S., Tamura A., Uesugi J., Python M., 2011. Crustal diopsidites from the northern Oman ophiolite: Evidence for hydrothermal circulation through suboceanic Moho. Journal of Mineralogical and Petrological Sciences 106, 261-266.

Akizawa N. and Arai S., 2014. Petrology of mantle diopsidite from Wadi Fizh, northern Oman ophiolite: Cr and REE mobility by hydrothermal solution. Island Arc 23, 312-323.

Alt J.C., Shank W.C., Jackson M.C., 1993. Cycling of sulfur in subduction zones: The geochemistry of sulfur in the Mariana Island Arc and back-arc trough. Earth and Planetary Science Letters 118, 477-494.

Antignano A. and Manning C.E., 2008. Rutile solubility in H2O, H_2O-SiO_2, and H_2O-$NaAlSi_3O_8$ fluids at 07-20 GPa and 700-1000 °C: implications for mobility of nominally insoluble elements. Chemical Geology 255, 283-293.

Arai S. and Akizawa N., 2014. Precipitation and dissolution of chromite by hydrothermal solutions in the Oman ophiolite: New behavior of Cr and chromite. American Mineralogist 99, 28-34.

Arndt N.T., 2008. Komatiite. Cambridge, Cambridge University Press, 467 p.

Bagheri S., 2007. The exotic Paleo-Tethys terrane in Central Iran: New geological data from Anarak, Jandaq and Posht-e-Badam areas. PhD thesis, Faculty of Geosciences and Environment, university of Lausanne, Switzerland, 208 p.

Bagheri S. and Stampfli G.M., 2008. The Anarak, Jandaq and Posht-e-Badam metamorphic complexes in central Iran: New geological data, relationships and tectonic implications. Tectonophysics 451, 123-155.

Barker F. and Arth J.G., 1976. Generation of trondhjemitic-tonalitic liquids and Archean bimodal trondhjemite-basalt suites. Geology 4, 596-600.

Barker F., 1979. Trondhjemite: Definition, environment and hypotheses of origin. In Barker F. (Ed.) Trondhjemites, Dacites and Related Rocks. Elsevier, Amsterdam, 1-12.

Ballard R.D., Francheteau J., Juteau T., Rangan C., Normark W., 1981. East Pacific rise at 21° N: the volcanic, tectonic and hydrothermal processes of the central axis. Earth and Planetary Science Letters 55, 1-10.

Becker H., Jochum K.P., Carlson R.W., 2000. Trace element fractionation during dehydration of eclogites from high-pressure terranes and the implications for element fluxes in subduction zones. Chemical Geology 163, 65-99.

Berger J., Femenias O., Mercier J.C.C., Demaiffe D., 2005. Ocean-floor hydrothermal metamorphism in the Limousin ophiolites (western French Massif Central): Evidence of a rare preserved Variscan oceanic marker. Journal of metamorphic Geology 23, 795-812.

Bosch D., Jamais M., Boudier F., Nicolas A., Dautria J.M., Agrinier P., 2004. Deep and hightemperature hydrothermal circulation in the Oman ophiolite - Petrological and isotopic evidence. Journal of Petrology 45, 1181-1208.

Capedri S., Garuti G., Rossi A., 1978. Rodingites from Pindos, Constraints on the "rodingite" problem. Neues Jahrbuch für Mineralogie Abhandlungen 132, 242-263.

Condie K.C., 1989. Geochemical changes in basalts and andesites across the Archean-Proterozoic boundary: Identification and significance. Lithos 23, 1-18.

Coogan L.A., Wilson R.N., Gillis K.M. MacLeod C.J., 2001. Near-solidus evolution of oceanic gabbros: insights from amphibole geochemistry. Geochimica et Cosmochimica Acta 65, 4339-4357.

Coolican C.T., Ansdell K.M., Kerrich R., Stauffer M., 2000. Geochemical character of the Tonalite-Trondhjemite suite of the Tonalite- Migmatite Complex, Deception Lake, Saskatchewan: in Summary of Investigations, vol. 2, Saskatchewan Geological Survey, Saskatchewan Energy and Mines, Miscellaneous report 2000-4.2, 86-94.

Crane K., Aikman F., Foucher J.P., 1988. The distribution of geothermal fields along the East Pacific Rise from 13°10′ N to 8°20′ N: implications for deep seated origins. Marine Geophysical Researches 9, 211-236.

Davis E.E. and Elderfield H., 2004. Hydrogeology of the Oceanic Lithosphere. Cambridge University Press, New York, 339-377.

Deer W.A., Howie R.A., Zussman J., 1992. An Introduction to the Rock-Forming Minerals. Longmans, 528 p.

Diefenbach W., Davoudzadeh K., Alavi-Tehrani M., Lensch G., 1986. Paleozoic Ophiolites of Iran, geology, geochemistry and geodynamic implication. Ofioliti 11, 305-338.

Droop G.T.R., 1987. A general equation for estimating Fe3+ concentrations in ferromagnesian silicates and oxides from microprobe analyses, using stoichiometric criteria. Mineralogical Magazine 51, 431-435.

Drummond M.S. and Defant M.J., 1990. A model for trondhjemite-tonalite-dacite genesis and crustal growth via slab melting: Archean to modern comparisons. Journal of Geophysical Research 95, 21503-21521.

Ferrando S., Luce Frezzotti M., Orione P., Carlo Conte R., Compagnoni R., 2010. Late-Alpine rodingitization in

the Bellecombe meta-ophiolites (Aosta Valley, Italian Western Alps): Evidence from mineral assemblages and serpentinization-derived H2-bearing brine. International Geology Review 52, 1220-1243.

Fouquet Y., 1997. Where are the large hydrothermal sulphide deposits in the oceans? Philosophical Transactions of the royal society, Mathematical, Physical and Engineering Sciences 355, 427-441.

Gregory R.T. and Taylor H.P., 1981. An oxygen isotope profile in a section of cretaceous oceanic crust, Samail ophiolite, Oman: evidence for δ180 buffering of the oceans by deep (<5 km) seawater-hydrothermal circulation at mid-ocean ridges. Journal of Geophysical research 86, 2737-2755.

Halama R., Wenzeli T., Upton B.G.J., Siebel W., Markl G., 2003. A geochemical and Sr-Nd-O isotopic study of the Proterozoic Eriksfjord Basalts, Gardar Province, South Greenland: Reconstruction of an OIB signature in crustally contaminated rift-related basalts. Mineralogical Magazine 67, 831-853.

Hanyu T., Tatsumi Y., Nakai S., Chang Q., Miyazaki T., Sato K., Tani K., Shibata T., Yoshida T., 2006. Contribution of slab melting and slab dehydration to magmatism in the NE Japan arc for last 25 Myr: constraints from geochemistry. Geochemistry Geophysics Geosystems 7, 1-29.

Harper G.D., 1985. Tectonics of slow spreading mid-ocean ridges and consequences of a variable depth to the brittle/ductile transition. Tectonics 4, 395-409.

Hart S.R., Blusztajn J., Dick H.J.B., Meyer P.S., Muehlenbachs K., 1999. The fingerprint of seawater circulation in a 500-meter section of ocean crust gabbros. Geochimica et Cosmochimica Acta 63, 4059-4080.

Henry D.J., Guidotti V.C., Thomson A.J., 2005. The Ti-saturation surface for low to medium pressure metapelitic biotites: Implications for geothermometry and Ti-substitution mechanisms. American Mineralogist 90, 316-328.

Hey M.H., 1954. Nomenclature of chlorites. Mineralogical Magazine, 277p.

Ishikawa T., Fujisawa S., Nagaishi K., Masuda T., 2005. Trace element characteristics of the fluid liberated from amphibolite-facies slab: Inference from the metamorphic sole beneath the Oman ophiolite and implication for boninite genesis. Earth and Planetary Science Letters 240, 355-377.

Kawahata H., Nohara M., Ishizuka H., Hasebe S., Chiba H., 2001. Sr isotope geochemistry and hydrothermal alteration of the Oman ophiolite. Journal of Geophysical Research 106, 11083-11099.

Kimball K.L., 1988. High temperature hydrothermal alteration of ultramafic cumulates from the base of the sheeted dykes in the Josephine ophiolite, NW California. Journal of Geophysical Research 93, 4675-4687.

Kolb M., Vonquadt A., Peytcheva I., Heinrich C.A., Fowler S.J., Cvetkovic V., 2013. Adakite-like and Normal Arc Magmas: Distinct Fractionation Paths in the East Serbian Segment of the Balkan-Carpathian Arc. Journal of Petrology 54, 421-451.

Koutsovitis P., Magganas A., Pomonis P., 2008. Rodingites within scattered ophiolitic occurrences from the northern and eastern Othris area, Greece. Proceedings of the 13th International Conference on Thermobaro-geochemistry and 5th APIFIS symposium 1, 243-246.

Lanphere M.A., 1981. K-Ar ages of metamorphic rocks at the base of the Samail ophiolite, Oman. Journal of Geophysical Research 86, 2777-2782.

Leake B.E., Woolley A.R., Arps C.E.S., Birch W.D., 1997. Nomenclature of amphiboles: Report of the subcommittee on amphiboles of the international mineralogical association, commission on new minerals and mineral names. The Canadian Mineralogist 35, 219-246.

Le Bas M.J., 1962. The role of aluminium in igneous clinopyroxenes with relation to their parentage. American Journal of Science 260, 267-288.

Le Maitre R.W., Bateman P., Dudek A., Keller J., Lameyre J., Le Bas M. J., Sabine P. A., Sorensen H., Streckeisen A., Wolley A. R., Zanetin B., 1989. A Classification of Igneous Rocks and Glossary of Terms. Recommendations of the IUGS Subcommision on the Systematics of Igneous Rocks. Oxford, Blackwell Scientific Publications, 193 pp.

Leterrier J., Maury R.C., Thonon P., Girard D., Marehal M., 1982. Clinopyroxene composition as a method of identification of the magmatic affinities of paleo-volcanic series. Earth and Planetary Science Letters 59, 139-154.

Li X.P., Zhang L.F., Wilde S.A., Song B., Liuet X.-M., 2010. Zircons from rodingite in the western Tianshan serpentinite complex: mineral chemistry and U-Pb ages define nature and timing of rodingitisation. Lithos 118, 17-34.

Martin H., Smithies R.H., Rapp R., Moyen J.F., Champion D., 2005. An overview of adakite, tonalite-trondhjemite-granodiorite (TTG), and sanukitoid: relationships and some implications for crustal evolution. Lithos 79, 1-24.

McCulloch M.T., Gregory R.T., Wasserburg G.J., Taylor H.P., 1981. Sm-Nd, Rb-Sr and 18O/16O isotopic systematic in an oceanic crust: Thermodynamic models of hydrothermal alteration. Journal of Geophysical Research 86, 2721-2735.

McCollom T.M. and Shock E.L., 1998. Fluid-rock interactions in the lower oceanic crust: Thermodynamic models of hydrothermal alteration. Journal of Geophysical Research 103, 545-575.

McDonough W.F. and Sun S.S., 1995. The composition of the Earth. Chemical Geology 120, 223-253.

Mollo S., Putirka K., Misiti V., Soligo M., Scarlato P., 2013. A new test for equilibrium based on clinopyroxene-melt pairs: clues on the solidification temperatures of Etnean alkaline melts at post-eruptive conditions. Chemical Geology 352, 92-100.

Mollo S., Blundy J., Scarlato P., De Cristofaro S.P., Tecchiato V., Di Stefano F., Vetere F., Holtz F., Bachmann O., 2018. An integrated P-T-H2O-lattice strain model to quantify the role of clinopyroxene fractionation on REE+Y and HFSE patterns of

mafic alkaline magmas: Application to eruptions at Mt. Etna. Earth-Science Reviews 185, 32-56.

Morimoto N., Fabrise J., Ferguson A., Ginzburg I.V., Ross M., Seifert F.A., Zussman J. Akoi K., Gottardi G., 1988. Nomenclature of pyroxenes. Mineralogical Magazine 52, 535-555.

Morishita T., Ishida Y., Arai S., 2005a. Simultaneous determination of multiple trace element compositions in thin (<30 μm) layers of BCR-2G by 193 nm ArF excimer laser ablation-ICP-MS: implications for matrix effect and elemental fractionation on quantitative analysis. Geochemical Journal 39, 327-340.

Morishita T., Ishida Y., Arai S., Shirasaka M., 2005b. Determination of multiple trace element compositions in thin (<30 μm) layers of NIST SRM 614 and 616 using laser ablation-inductively coupled plasma-mass spectrometry. Geostandards and Geoanalytical Research 29, 107-122.

Nachit H., Ibhi A., Abia E.H., Ohoud M.B., 2005. Discrimination between primary magmatic biotites, re-equilibrated biotites and neoformed biotites. Comptes Rendus Geoscience 337, 1415-1420.

Nimis P. and Vannucci R., 1995. An ion microprobe study of clinopyroxenes in websteritic and megacrystic xenoliths from Hyblean Plateau (SE Sicily, Italy): constraints on HFSE/REE/Sr fractionation at mantle depth. Chemical Geology 124, 185-197.

Nosouhian N., Torabi Gh., Arai S., 2019. Petrological aspects of the Bayazeh Paleozoic ophiolite (Central Iran); implications for Paleo-Tethys subduction. Periodico di Mineralogia 88, 105-134.

O'Hanley D.S., Schandl E.S., Wicks F.J., 1992. The origin of rodingites from Cassiar, British Columbia, and their use to estimate T and P (H_2O) during serpentinisation. Geochimica et Cosmochimica Acta 56, 97-108.

Python M., Ceuleneer G., Ishida Y., Barrat J.A., Arai S., 2007. Oman diopsidites: A new lithology diagnostic of very high temperature hydrothermal circulation in mantle peridotite below oceanic spreading centers. Earth and Planetary Science Letters 255, 289-305.

Python M., Yoshikawa M., Shibata T., Arai S., 2011. Diopsidites and rodingites: Serpentinisation and Ca-metasomatism in the Oman ophiolite mantle. Springer-Verlag Berlin Heidelberg, 401-435.

Ramseyer K., Boles J.R., Lichtner P.C., 1992. Mechanism of plagioclase albitization. Journal of Sedimentary Petrology 62, 349-356.

Rebay G., Riccardi M.P., Spalla M.I., 2015. Fluid rock interactions as recorded by Cl-rich amphiboles from continental and oceanic crust of italian orogenic belts. Periodico di Mineralogia 84, 751-777.

Ribeiro J.M., Maury R.C., Gre´goire M., 2016. Are Adakites Slab Melts or High-pressure Fractionated Mantle Melts? Journal of Petrology 1-24.

Rieder M., Cavazzini G., D'yakonov Y.S., Frank-Kamenetskii V.A., Gottardi G., Guggenheim S., Koval' P.V., Müller G., Neiva A.M.R., Radoslovich E.W., Robert J.L., Sassi F.P., Takeda H., Weiss Z., Wones D.R., 1998. Nomenclature of the micas. Canadian Mineralogist 36, 905-912.

Rizzo G., Laurita S., Altenberger U., 2018. The Timpa delle Murge ophiolitic gabbros, southern Apennines: insights from petrology, geochemistry and consequences to the geodynamic setting. Periodico di Mineralogia 87, 5-20.

Saccani E., Azimzadeh Z., Dilek Y., Jahangiri A., 2013. Geochronology and petrology of the Early Carboniferous Misho Mafic Complex (NW Iran), and implications for the melt evolution of Paleo-Tethyan rifting in Western Cimmeria. Lithos 162-163, 264-278.

Schandl E.S., O'Hanley D.S., Wicks F.J., 1989. Rodingites in serpentinized ultramafic rocks of the Abitibi greenstone belt, Ontario. Canadian Mineralogist 27, 579- 591.

Schandl E.S. and Mittwede S.K., 2001. Evolution of Acipayam (Denizli, Turkey) rodingites. International Geology Review, 3rd International Turkish Geology Symposium 43, 611-623.

Shand S.J., 1943. Eruptive Rocks: Their Genesis, Composition, Classification, and their Relations to Ore-deposits. Wiley, 444 p.

Sharokovski M., Susov M., Krivyakin B., Morozov L., Kiristaev V., Romanko E., 1984. Geology of the Anarak area (Central Iran). Geological Survey of Iran 19, 143 p.

Spear F.S., 1981. An experimental study of hornblende stability and compositional variability in amphibolite. American Journal of Science 281, 697-734.

Stalder R., Foley S., Brey G.P., Horn I., 1998. Mineral aqueous fluid partitioning of trace elements at 900-1200 °C and 3.0-5.7 GPa: new experimental data for garnet, clinopyroxene and rutile and implications for mantle metasomatism. Geochimica et Cosmochimica Acta 62, 1781-1801.

Stampfli G.M. and Borel G.D., 2004. The TRANSMED transects in space and time: constraints on the paleotectonic evolution of the Mediterranean domain. In: Cavazza, W., Roure, F., Spakman, W., Stampfli, G.M., Ziegler, P. (Eds.), The TRANSMED Atlas: the Mediterranean Region from Crust to Mantle. Springer Verlag, 53-80.

Sun S.S.and McDonough W.F., 1989. Chemical and isotopic systematics of oceanic basalts: implications for mantle composition and processes, in magmatism in Ocean Basins, Saunders A.S. and Norry M.J., Eds., Geological Society, London, Special Publications 42, 313-345.

Sun C. and Liang Y., 2012. Distribution of REE between clinopyroxene and basaltic melt along a mantle adiabat: Effects of major element composition, water, and temperature. Contributions to Mineralogy and Petrology 163, 807-823.

Tatsumi Y., 2000. Continental crust formation by crustal delamination in subduction zones and complementary accumulation of the enriched mantle I component in the mantle, Geochemistry Geophysics Geosystems 1, Paper

number 2000GC000094.

Torabi G., 2009. Chromitite potential in mantle peridotites of the Jandaq ophiolite (Isfahan province, Central Iran). Comptes Rendus Geoscience 341, 982-992.

Torabi G., 2011. Late Permian blueschist from Anarak ophiolite (Central Iran, Isfahan province), a mark of multi-suture closure of the Paleo-Tethys Ocean. Revista Mexicana de Ciencias Geologicas 28, 544-554.

Torabi G., Shirdashtzadeh N., Arai S., Koepke J., 2011. Paleozoic and Mesozoic ophiolites of Central Iran: amphibolites from Jandaq, Posht-e-Badam, Nain and Ashin ophiolites. Neues Jahrbuch für Geologie und Paläontologie 262, 227-240.

Torabi G., 2012. Late Permian post-ophiolitic trondhjemites from Central Iran: A mark of subduction role in growth of Paleozoic continental crust. Island Arc 21, 215-229.

Torabi G., 2013. Chromitite absence, presence and chemical variety in ophiolites of the Central Iran (Naein, Ashin, Anarak and Jandaq). Neues Jahrbuch Für Geologie Und Paläontologie - Abhandlungen 267, 171-192.

Torabi G., Arai S., Morishita T., Tamura A., 2017. Mantle Hornblendites of Naein Ophiolite (Central Iran): Evidence of deep high temperature hydrothermal metasomatism in an upper mantle section. Petrology 25, 114-137.

Tribuzio R., Renna M.R., Dallai L., Zanetti A., 2014. The magmatic-hydrothermal transition in the lower oceanic crust: Clues from the Ligurian ophiolites, Italy. Geochimica et Cosmochimica Acta 130, 188-211.

Tsikouras B., Karipi S., Rigopoulos I., Perraki M., Pomonis P., Hatzipanagiotou K., 2009. Geochemical processes and petrogenetic evolution of rodingite dykes in the ophiolite complex of Othrys (Central Greece). Lithos 113, 540-554.

Tsygankov A.A., Udoratina O.V., Burmakina G.N., Antsiferova T.N., Coble M.A., 2016. The Early Paleozoic basite magmatism of Western Transbaikalia: composition, isotope age (U-Pb, SHRIMP RG), magma sources, and geodynamics, Petrology 24, 367-391.

Veblen D.R. and Ribbe P.H., 1982. Amphiboles; Petrology and experimental phase relations, Mineralogical Society of America. Reviews in Mineralogy 9B, 390 p.

Wang Q., Wyman D.A., Xu J.F., Wan Y., Li C.H., Zi F., Jiang Z., Qiu H., Chu Zh., Zhao Z.H., Dong Y.H., 2007. Triassic Nb-enriched basalts, magnesian andesites, and adakites of the Qiangtang terrane (Central Tibet): evidence for metasomatism by slab-derived melts in the mantle wedge. Contributions to Mineralogy and Petrology 155, 473-490.

Winchester J.A. and Floyd P.A., 1977. Geochemical Discrimination of Different Magma Series and Their Differentiation Product Using Immobile Elements. Chemical Geology 20, 325-343.

Whitney D.L. and Evans B.W., 2010. Abbreviations for names of rock-forming minerals. American Mineralogist 95, 185-187.

Wood B.J. and Blundy J.D., 1997. A predictive model for rare earth element partitioning between clinopyroxene and anhydrous silicate melt. Contributions to Mineralogy and Petrology 129, 166-181.

Zanchi A., Zanchetta S., Garzanti E., 2009. The Cimmerian evolution of the Nakhlak-Anarak area, Central Iran, and its bearing for the reconstruction of the history of the Eurasian margin, In Brunet M.F., Wilmsen M., Granath J.W., (Eds.) SouthCaspian to Central Iran Basins. Geological Society, London, Special Publications 312, 261-286.

Zhang H., Niu H., Sato H., Yu X., Shan Q., Zhang B., Ito J., Nagao T., 2005. Late Paleozoic adakites and Nb-enriched basalts from northern Xinjiang, northwest China: Evidence for the southward subduction of the Paleo-Asian Oceanic Plate. Island Arc 14, 55-68.